PTR-MS MOBILE LABORATORY VAPOR MONITORING MONTHLY REPORT – MONTH 4

Report No. 53005-81-RPT-039
Revision 0
November 12, 2018 – December 31, 2018

Prepared for:

Washington River Protection Solutions, LLC
P.O. Box 850
Richland, WA 99352

Subcontract 53005, Release 81

Prepared by:
TerraGraphics Environmental Engineering, Inc.
2926 E. Ainsworth St.
Pasco, WA 99301

www.terragraphics.com

Approval Form

Prepared by:

Tyler Williams Date: 10/22/2019
Tyler Williams

Reviewed by:

Date: 10/22/2019
Matthew Erickson, Ph.D.

Approved by:

Date: 10/22/2019
Rich Westberg

Record of Revision

Revision	Date	Pages/Sections Changed	Brief Description
0	10/2019	All	Original Issue.

Table of Contents

Figures

Tables

Acronyms and Abbreviations

ASTM	ASTM International, Inc.
COPC	Chemical of Potential Concern
DR	Deficiency Report
GPS	Global Positioning System
IH	Industrial Hygiene
IP	Ionization Potential
MDL	Method Detection Limit
ML	Mobile Laboratory (Mobile Vapor Monitoring Laboratory)
MW	Molecular Weight
NDMA	N-Nitrosodimethylamine
NIOSH	National Institute for Occupational Safety and Health
OSC	Organosulfur Compound
ppbv	parts per billion by volume
ppmv	parts per million by volume
pptv	parts per trillion by volume
PTR-MS	Proton Transfer Reaction – Mass Spectrometer
PTR-TOF	Proton Transfer Reaction – Time of Flight
SME	Subject Matter Expert
SRI-MS	Selective Reagent Ionization – Mass Spectrometer
Td	Townsend
TOF-MS	Time of Flight – Mass Spectrometer
VOC	Volatile Organic Compound

Executive Summary

In support of the Hanford Vapor Monitoring, Detection, and Remediation Project, Washington River Protection Solutions, LLC has subsidized the implementation of a mobile vapor monitoring laboratory developed by TerraGraphics Environmental Engineering, Inc. (Statement of Work #306312, “Mobile Laboratory Services and Lease”). The contract secures services associated with the lease and operation of the Mobile Laboratory designed specifically for trace gas analysis based on the Proton Transfer Reaction – Mass Spectrometer and supplemental analytical instruments. Operation of the Mobile Laboratory will be at the discretion of Washington River Protection Solutions, LLC and will be conducted to support a variety of projects including continuing background studies, fugitive emissions, waste disturbing activities, leading indicator studies, and general area sampling. Other applications of the Mobile Laboratory will be determined as needed by Washington River Protection Solutions, LLC.

This report of Month 4 operations spans the calendar months of November 2018 and December 2018, specifically November 12, 2018, through December 31, 2018. Combining this period into a single monthly report is logical due to delayed start from a background study (Month 3) which ran into early November 2018 along with a period of time off for holidays.

During Month 4, stack monitoring of the AP Tank Farm stack occurred. During the AP Stack Operational Acceptance Test, ammonia was to be injected into the stack monitor cell at a variety of concentrations. This caused a slight increase in ammonia concentration emitted from the stack during this time. The Mobile Laboratory monitored ammonia concentrations downwind of AP Stack before, during, and after elevated ammonia releases.

Source characterization of the septic tanks near the 242A Evaporator was conducted in support of the Fugitive Emissions Team.

Maintenance, modifications, verifications, and calibrations were performed on the Mobile Laboratory instrumentation for the remainder of Month 4.

1.0 DESCRIPTION OF TESTS CONDUCTED

During Month 4, spanning the dates of November 12, 2018, to December 31, 2018, the Mobile Laboratory (ML) was deployed to monitor chemicals of potential concern (COPCs) and to characterize sources of potential odor-causing compounds on the Hanford Site.

The ML was deployed to AP Tank Farm in the 200 East area of the Hanford Site to monitor the ammonia releases from AP Stack from November 19, 2018, to November 20, 2018. The ML was used to monitor the septic tanks located east of the 242A Evaporator on the Hanford Site for one day during Month 4.

Description of activities that were conducted are as follows:

- Week 15
    - Maintenance and AP Stack Monitoring
- Week 16
    - Maintenance and AP Stack Monitoring
- Week 17
    - Maintenance and Septic Source Characterization
- Week 18
    - Maintenance, Modifications, and Testing
- Week 19
    - Maintenance, Modifications, and Testing
- Week 20
    - Maintenance, Modifications, and Testing
- Week 21
    - Maintenance, Modifications, and Testing

Beyond monitoring, the tasks conducted during this period were performed to support proper function of the instruments in the ML. These tasks include calibrations, troubleshooting, verifications, and maintenance.

This report is structured based on reporting requirements, as defined in the original statement of work.

2.0 MEASUREMENT SYSTEM DESIGN

This section describes the sampling methods, instrumentation, and confirmatory measurements used during this monitoring period.

2.1 Sampling Methods

2.1.1 Design of Sampling System

The ML is housed in a Chevrolet®[1] 4500 14' Box Truck equipped with a 5.2L diesel engine. The box has been fully insulated to allow the ML to maintain comfortable working temperatures for the Operators and the instrumentation. The ML has the option of utilizing either shore power or onboard diesel generator power for operation of the instruments. During Month 4, while the ML was located at the TerraGraphics warehouse in Pasco, WA, shore power was utilized. The ML was powered by the generator at all deployed locations during Month 4. When deployed for monitoring, the ML used both the mast and the side port to perform air sampling.

The layout of the ML and the sampling system is shown in the following drawings:

- 66409-18-ML-003, *Sampling Manifold Sketch*; and
- 66409-18-ML-004, *Mobile Lab Schematics*.

2.1.1.1 PTR-MS Sampling

Proton Transfer Reaction – Time of Flight (PTR-TOF) 6000 X2 is the latest trace Volatile Organic Compound (VOC) analyzer from IONICON®[2].

The PTR-TOF 6000 X2 is used to quantify COPCs from the sampled air. The sampled air enters the PTR drift tube. In the drift tube, VOCs undergo chemical ionization via a fast proton transfer reaction using the reagent ion, hydronium. The hydronium is produced from water vapor via a series of reactions in the hollow cathode PTR ion source. This is a soft ionization method and VOC fragmentation is minimized. These ionized compounds and hydronium then travel through the drift tube to the transfer lens system, subsequently entering the TOF-MS where they are separated by mass and monitored. The signal from the Time of Flight – Mass Spectrometer (TOF-MS) is used to identify the VOCs based on their mass, as well as to calculate individual compound concentration based on the ratio of compound signal to hydronium signal.

2.1.1.2 DAQFactory Sampling

DAQFactory®[3] is a data acquisition and automation software from AzeoTech that allows users to design custom applications with control and automatic output settings. In the ML, DAQFactory

---

[1] Chevrolet is a registered trademark of General Motors, LLC, Detroit, Michigan.
[2] IONICON is a registered trademark of Ionicon Analytik Gesellschaft m.b.H., Innsbruck, Austria.
[3] DaqFactory is a registered trademark of AzeoTech, Inc., Ashland, Oregon.

controls the sampling system through valves and flow controllers for the LI-COR®[4] CO_2 monitor, Picarro Ammonia Analyzer, AirMar®[5] Weather Station, and the PTR-TOF.

2.2 Instrumentation and Methods Used

2.2.1 Proton Transfer Reaction Mass Spectrometer

Measurements performed by the ML during Fiscal Year 2018 utilized the IONICON PTR-TOF 6000 X2 system. The mass resolution of the PTR-TOF 6000 is sufficient to resolve some COPCs with high confidence (i.e., furan from isoprene) while other compounds have interferences which can potentially compromise their reliable detection and quantification. A full discussion of the reliability of COPC detection and quantification as performed by a PTR-TOF 4000, an instrument with less resolution, can be found in *Fiscal Year 2017 Mobile Laboratory Vapor Monitoring at the Hanford Site: Monitoring During Waste Disturbing Activities and Background Study*, September 2017. A brief summary of the instrument and its underlying chemistry that leads to the sensitive detection of vapor components will be provided herein. The general layout of the instrument is shown in Figure 2-1.

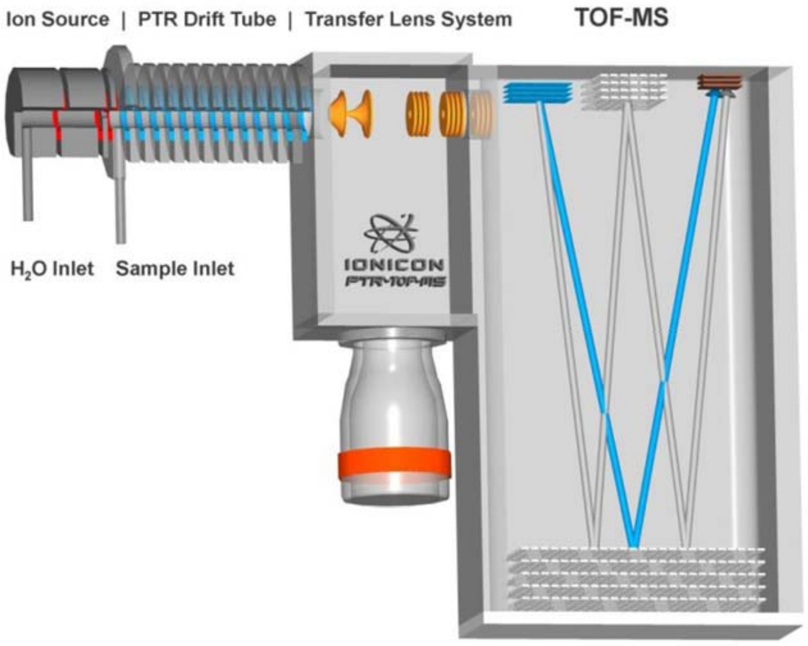

Figure 2-1. The General Configuration of an IONICON PTR-TOF Instrument.

The VOCs are measured by chemical ionization, where the reagent ion H_3O^+ ionizes organics via a fast proton transfer reaction (R1).

$$R + H_3O^+ \rightarrow RH^+ + H_2O \qquad \text{(R1)}$$

---

[4] LI-COR is a registered trademark of LI-COR, Inc., Lincoln, Nebraska.
[5] Airmar is a registered trademark of Airmar Technology Corporation, Milford, New Hampshire.

These reactions are normally non-dissociative, although there are some compounds that fragment to smaller ions upon protonation. The reaction takes place in a drift tube where the sample air stream reacts with H_3O^+ ions produced by a hollow cathode ion source. The number of ions counted per second for the reagent ion and protonated sample ion are monitored and used for the determination of estimated concentrations according to Equation 1.

$$[R] = \frac{1}{kt}\left(\frac{I_{RH+}}{I_{H3O+}}\right)\frac{\varepsilon_{RH+}}{\varepsilon_{H3O+}} \tag{1}$$

where k is the ion–molecule rate constant (molecules cm^{-3} s^{-1}), t is the reaction time (~ 100 microseconds), I_{RH+} and I_{H3O+} are the respective ion count rates, and ε_{RH+} and ε_{H3O+} are the ion transmission efficiencies through the TOF. It is important to note that estimated concentrations of compounds can be determined directly from Equation 1 (the "kinetic approach" to quantification). There is no need for the analysis of authentic standards and the generation of calibration curves. The system is essentially self-correcting as all measurements are made with respect to the ion count rate of the reagent ion.

The mixing ratio X of the organic R in the sample air is then determined by:

$$X_R\ (ppbV) = \frac{[R]}{[AIR]_{drift}} \times 1 \times 10^9 \tag{2}$$

where *[AIR]* is the number density of air (molecules/cm^3) in the drift tube given the drift tube pressure (typically ~ 2.4 mbar) and temperature (typically ~ 50°C).

The Proton Transfer Reaction – Mass Spectrometer (PTR-MS) technology has been used in numerous applications around the world with hundreds of peer-reviewed publications appearing in the literature over the past 20 years. Even though the technology is widely used in the research arena and has proven to be indispensable for many applications, there is no standard method among the United States regulatory agencies such as the U.S. Environmental Protection Agency, American Society for Testing and Materials (ASTM)®[6], and National Institute for Occupational Safety and Health (NIOSH)®[7]. The end user of the technology is expected to provide the "best practice" in its use by adhering to established operational parameters governed by the scope of the project and the nature of the sample(s) to be measured.

The kinetic approach provides quantitative estimates based on the use of relative ion signals of target compounds versus that of the reagent ion with an applied reaction rate constant found in the literature. This approach was chosen over the use of calibration standards due to the challenges associated with obtaining stable calibration mixtures for the Hanford COPC list. All quantification performed in this report was accomplished by the kinetic approach.

---

[6] ASTM is a registered trademark of American Society for Testing and Materials, West Conshohocken, Pennsylvania.
[7] NIOSH is a registered trademark of U.S. Department of Health and Human Services, Bethesda, Maryland.

2.2.2 Carbon Dioxide Monitor

Carbon dioxide is not a COPC; however, monitoring CO_2 is necessary for correlation of vapor signals to combustion processes or other sources. There are numerous combustion sources near the sampling sites of Month 4 including diesel and gas generators, all-terrain vehicles with no catalytic converters, and diesel and gasoline vehicles. These contribute VOCs to the vapor burden and are readily observed by the PTR-MS. It is necessary to distinguish these VOCs from tank farm related emissions resulting from normal work-related activities.

The CO_2 monitor used in the TerraGraphics ML was the LI-COR Model 840A. The Li-840A is an absolute, non-dispersive infrared gas analyzer based upon a single path, dual wavelength infrared detection system. It is a low-maintenance, high-performance monitoring solution that gives accurate, stable readings over a wide range of environmental conditions. It has a range of 0-20,000 ppm (0-2%), low power consumption (4W after power-up), and 1-second signal averaging to allow for real-time source apportionment (i.e., monitoring vehicle exhaust or other combustion sources on the fly). The instrument operates on a gas flow of less than 1 liter per minute.

It is interfaced to the ML's internal gas manifold at the same location as the PTR-MS sampling port to ensure that both instruments are simultaneously measuring the same source. The data from the CO_2 monitor are used to predict when VOC measurements from the PTR-MS come from combustion sources.

The CO_2 monitor used during Month 4 was operated using a factory calibration. Periodic checks of the unit were made with zero air and ambient background air [ambient atmospheric CO_2 levels are approximately 400 parts per million by volume (ppmv)], and a certified reference standard to ensure continued system operation. The system has a continuous direct readout which can be displayed on the DAQFactory monitor in real time to aid in real-time decision making by the field analysts.

2.2.3 Ammonia Monitor

Ammonia is a compound on the COPC list of particular importance. It is believed to be associated with all high-level waste storage tanks on the Hanford Site. The global average background for ammonia is between 5-7 parts per billion by volume (ppbv). Previous studies of ammonia levels on the Hanford Site indicate the expected measurement range should be in the low ppbv range. Although relatively easy to measure at the parts per million by volume (ppmv) level, its measurement at the low ppbv level with high temporal resolution is not trivial. The purpose of measuring trace levels of NH_3 is the correlation of vapor data from the PTR-MS to actual tank emissions. A measured vapor plume containing elevated COPCs with the same time correlation as an ammonia plume is reasonable evidence of a tank emission.

The ammonia monitor used was a Picarro Model G2103 that is capable of measuring NH_3 with parts per trillion by volume (pptv) sensitivity. It is a sophisticated time-based measurement system that uses a laser to quantify spectral features of gas phase molecules in an optical cavity. It is based on cavity ring down spectroscopy. Gas phase spectroscopy measurements are subject to temperature and pressure fluctuations. The Picarro system features a ± 0.005°C temperature stability and ± 0.0002 atm pressure stability to ensure low noise and high accuracy measurements. Sample flow rate to the instrument was provided by an external pump at 0.8 liters per minute at 760 Torr.

The analyzer is interfaced to the ML main sample stream to ensure the instrument measured the same gas sample as the PTR-MS and CO_2 monitor. The system outputs real-time data to a monitor, records data to its internal computer, and uses the ML Wi-Fi connection to automatically synchronize to a clock service. Daily data sets are retrieved and backed up similar to the other data collection instruments.

2.2.4 Weather Station

The weather station used in the ML is an Airmar 200WX-IPx7 with a control unit mounted in the server cabinet and the transducer mounted on the sampling mast located above the roof of the van. Real-time display of the output is visible on the DAQFactory monitor to aid field analysts in making sampling decisions in the field. The output data are fed to the server with a clock time-stamp that is synchronized to the other monitoring systems in the laboratory. The functions and outputs of the station include:

- Apparent wind speed and angle,
- True wind speed and angle,
- Air temperature,
- Barometric pressure,
- 2D Magnetic compass heading,
- Heading relative to true north, and
- Global positioning system (GPS).

The weather station transmitted data continuously at 2-second intervals to DAQFactory.

2.3 Confirmatory Measurements (If Applicable)

During Month 4, no confirmatory samples were taken.

3.0 CALIBRATION METHODS AND CALIBRATION GASES USED

Table 3-1. Calibrated Gases in Use During Month 4.

Cylinder	ID#	Exp. Date
Carbon Dioxide	77-401243203-1	07/13/2026
Ammonia	48-401233442-1	06/21/2019
Zero-air	Lot #: 2181802 (115421, C5438107, T-2768, 330-662, KI428)	06/29/2019
VOC	160-401265983-1	02/28/2019
Furan	CC707581	02/18/2019
N-Nitrosodimethylamine	CC496322	02/24/2019
1,3-butadiene	CC508261	03/06/2019

4.0 MEASUREMENT UNCERTAINTY AND KNOWN SOURCES OF ERROR

4.1.1 Proton Transfer Reaction – Mass Spectrometer

All standards/zeroes performed by the field team to verify the accuracy of the instrument fell within acceptable administrative limits as described in 66409-RPT-004, *Mobile Laboratory Operational Procedure*.

4.1.2 Carbon Dioxide Monitor

The LI-COR CO_2 Analyzer had no specific errors associated within the timeframe covered in this monthly report. All standards/zeroes performed by the field team and reported in this summary to verify the accuracy of the instrument fell within acceptable administrative limits (± 20%). The measurement accuracy of a properly calibrated instrument is listed in the LI-COR factory specifications as ±3% of reading.

4.1.3 Ammonia Monitor

The Picarro G2103 Ammonia Monitor had no specific errors associated within the timeframe covered in this monthly report. Further detail regarding the errors associated with measuring ammonia using a Picarro instrument is discussed in *Fiscal Year 2017 Mobile Laboratory Vapor Monitoring at the Hanford Site: Monitoring During Waste Disturbing Activities and Background Study*, September 2017. All standards/zeroes associated with data reported in this summary performed by the field team to verify the accuracy of the instrument fell within acceptable administrative limits (±20). The measurement accuracy of a calibrated instrument listed in the Picarro factory specifications is ±5% of reading.

4.1.4 Weather Station

The AirMar 200WX-IPx7 Weather Station had no specific errors associated within the timeframe covered in this monthly report. The Airmar 150 WX Weather Station is factory calibrated and is not user calibrated. The manual does not recommend periodic calibration. This is described in 66409-RPT-003, *Mobile Laboratory Operational Acceptance Testing Plan*.

4.2 Method Detection Limit

In order to gain insight into the limits of detection of the PTR-TOF 6000 X2, all zero-air checks run on the instrument from November 12, 2018, to December 31, 2018, were analyzed. A total of 15 zero-air checks were run during this time period. Each zero-air check consisted of roughly 100 data points, taken at 2 Hz. This period in particular was chosen because it takes into account improvements to performance and instrument tuning achieved as a result of the findings of DR-018-009, where high instrument background signals were observed at a variety of m/z. The tuning achieved during Month 3 after corrective action was taken still held true for Month 4 activities; therefore, the method detection limits (MDLs) obtained in Month 3 are still applicable to this report and were not recalculated.

The MDLs were calculated by taking the mean and standard deviation of the data collected during each zero-air check, for each compound detected. This takes into account the variance (or noise) present in the real-time data.

$$\mu = \frac{\sum_{i=1}^{n} x_i}{n}$$

$$\sigma = \sqrt{\frac{\sum_{i=1}^{n}(x_i - \mu)^2}{n}}$$

Next, a grand mean of the mean values for each zero-air check for each compound was calculated by taking the mean of the 15 individual means calculated in the previous step.

$$\mu_T = \frac{\sum_{i=1}^{n} \mu_i}{n}$$

Using propagation of error, the standard deviations were combined. This was done by taking the square root of the average of the squares of each calculated standard deviation, i.e., the root of the average of the variances.

$$\sigma_T = \sqrt{\frac{\sum_{i=1}^{n} \sigma_i^2}{n}}$$

This ensured that the variances attributed to the discrete points of 2 Hz data were conserved. If a standard deviation of the mean of means was taken, the only variance taken into account would be the variance between calculated averages.

These combined standard deviations were then multiplied by the 2-tailed Student's t-value for 14 degrees of freedom at 95% CI, i.e., 2.15. This provided the MDLs for each compound detected by the PTR-TOF 6000 X2. As a conservative approach, an additional factor of three was then applied to the MDLs to obtain the reporting limits (RLs). Calculated MDLs and RLs for each COPC and odor compound are shown in the table below.

Table 4-1. Method Detection Limits and Reporting Limits for Chemicals of Potential Concern. (2 Sheets)

COPC Name	OEL (ppbv)	MDL (ppbv)	RL (ppbv)
formaldehyde	300	0.035	0.105
methanol	200000	0.051	0.152
acetonitrile	20000	0.004	0.013
acetaldehyde	25000	0.035	0.106
ethylamine	5000	0.004	0.011
1,3-butadiene	1000	0.010	0.031
propanenitrile	6000	0.005	0.015
2-propenal	100	0.025	0.075
1-butanol + butenes	20000	0.011	0.034
methyl isocyanate	20	0.005	0.016
methyl nitrite	100	0.004	0.013
furan	1	0.004	0.012
butanenitrile	8000	0.003	0.008
but-3-en-2-one + 2,3-dihydrofuran + 2,5-dihydrofuran	200, 1, 1	0.003	0.009
butanal	25000	0.005	0.016
NDMA	0.3	0.004	0.013
benzene	500	0.018	0.053
2,4-pentadienenitrile + pyridine	300, 1000	0.005	0.014
2-methylene butanenitrile	30	0.002	0.007
2-methylfuran	1	0.003	0.010
pentanenitrile	6000	0.002	0.007
3-methyl-3-buten-2-one + 2-methyl-2-butenal	20, 30	0.004	0.011
NEMA	0.3	0.003	0.008
2,5-dimethylfuran	1	0.003	0.009
hexanenitrile	6000	0.002	0.005
2-hexanone (MBK)	5000	0.004	0.011
NDEA	0.1	0.002	0.007
butyl nitrite + 2-nitro-2-methylpropane	100, 300	0.003	0.010
2,4-dimethylpyridine	500	0.003	0.008
2-propylfuran + 2-ethyl-5-methylfuran	1	0.002	0.007
heptanenitrile	6000	0.002	0.005
4-methyl-2-hexanone	500	0.003	0.008

Table 4-1. Method Detection Limits and Reporting Limits for Chemicals of Potential Concern. (2 Sheets)

COPC Name	OEL (ppbv)	MDL (ppbv)	RL (ppbv)
NMOR	0.6	0.002	0.007
butyl nitrate	2500	0.002	0.005
2-ethyl-2-hexenal + 4-(1-methylpropyl)-2,3-dihydrofuran+ 3-(1,1-dimethylethyl)-2,3-dihydrofuran	100, 1, 1	0.002	0.006
6-methyl-2-heptanone	8000	0.002	0.006
2-pentylfuran	1	0.002	0.007
biphenyl	200	0.002	0.007
2-heptylfuran	1	0.004	0.011
1,4-butanediol dinitrate	50	0.004	0.011
2-octylfuran	1	0.001	0.004
1,2,3-propanetriol 1,3-dinitrate	50	0.003	0.010
PCB	1000	0.004	0.011
6-(2-furanyl)-6-methyl-2-heptanone	1	0.001	0.003
furfural acetophenone	1	0.003	0.008

Table 4-2. Method Detection Limits and Reporting Limits for Odor-Causing Compounds.

Odor Name	MDL	RL
methyl mercaptan	0.007	0.020
dimethyl sulfide; ethanethiol	0.005	0.014
allyl mercaptan	0.008	0.023
1-propanethiol; Isopropyl mercaptan	0.006	0.018
2-butene-1-thiol	0.005	0.014
Diethyl Sulfide; 2-methylpropane-2-thiol	0.031	0.094
thiopropanal sulfuroxide	0.008	0.024
dimethyl disulfide	0.006	0.017
1-pentanethiol; 2,2-dimethylpropane-1-thiol	0.005	0.016
benzenethiol	0.004	0.012
diallyl sulfide	0.003	0.009
methyl propyl disulfide	0.005	0.015
methylbenzenethiol	0.003	0.010
dimethyl trisulfide	0.003	0.009
(1-oxoethyl) thiophene	0.009	0.028
(1-oxopropyl) thiophene	0.004	0.012
dipropyl disulfide	0.003	0.008
methyl propyl trisulfide	0.004	0.012
dimethyl tetrasulfide	0.002	0.005
dipropyl trisulfide	0.003	0.008
diphenyl sulfide	0.002	0.006

It is worth noting that while the RLs are calculated with the purpose of applying them to the data in an effort to reduce the likelihood of false positives at low concentrations, these calculated RLs will not be applied retroactively to the data discussed in this monthly report.

5.0 TEST RESULTS

This section details the test results found during this month's monitoring activities.

5.1 Discussion of Test Activities and Observations – AP Stack

The ML was deployed on November 15, 2018, for a run-through at AP Stack and two days were focused on monitoring the ammonia releases from AP Stack, located in the AP Tank Farms on the Hanford Site. Table 5-1 lists the various activities conducted during mobile monitoring of AP Stack during Month 4.

Table 5-1. AP Tank Farm Stack Monitoring Activities.

Week	Date	Description	Activities/Observations
16	11/15/2018	Mobile Monitoring	AP Stack Site run-through with Mr. George Weeks
	11/19/2018	Mobile Monitoring	AP Stack ammonia releases
	11/20/2018	Mobile Monitoring	AP Stack ammonia releases

Table 5-2 lists the ammonia release time periods and concentrations. Varying concentrations were released within the stack with the release period being approximately 20 minutes. The objective of the ML was to remain downwind of the AP Stack to capture the ammonia concentrations within the stack emission plume. On November 15, 2018, the ML Operators worked with Mr. Weeks to run through the APGEMS program. This program models the AP Stack emission plume and predicts the potential dispersion. Running the program at regular intervals would allow the ML Operators to position the ML in appropriate locations downwind. On November 19, 2018, and November 20, 2018, there were multiple error messages that prevented use of the APGEMS software during the ammonia releases. The ML wind measurements were used to determine appropriate positioning of the ML.

Table 5-2. Time and Concentration of Ammonia Releases in the AP Stack.

Date	Start	Stop	ppmv
11/19/2018	13:05	13:25	0.6
11/19/2018	13:49	14:09	0.1
11/20/2018	9:43	9:59	1
11/20/2018	10:14	10:37	638
11/20/2018	12:18	12:37	330
11/20/2018	12:51	13:11	102
11/20/2018	13:31	13:49	0.346

Figure 5-1 shows the locations of the ML during the releases. The ML was located to other locations during the two ammonia release days, but was only at location A or B in Figure 5-1 during the releases.

Source: Esri, DigitalGlobe, GeoEye, Earthst
IGN, and the GIS User Community

Figure 5-1. AP Tank Farm Stack Monitoring.

5.2 Identification of Vapor Sources and Quantitative Analysis of Vapor Composition – AP Stack

There were two ammonia releases on November 19, 2018, at 13:05 and 13:40 at 0.6 ppmv and 0.1 ppmv of ammonia, respectively. The ML was positioned at Location A in Figure 5-1 for the 13:05 release and at Location B in Figure 5-1 for the 13:40 release. Figure 5-2 shows the ammonia concentration throughout the day accompanied by wind direction. There were no increases in ammonia observed for the entire monitoring period and the concentrations represented standard atmospheric background for the area. The times of the releases are signified by the red bars in Figure 5-2 and show that no changes in ammonia concentration occurred.

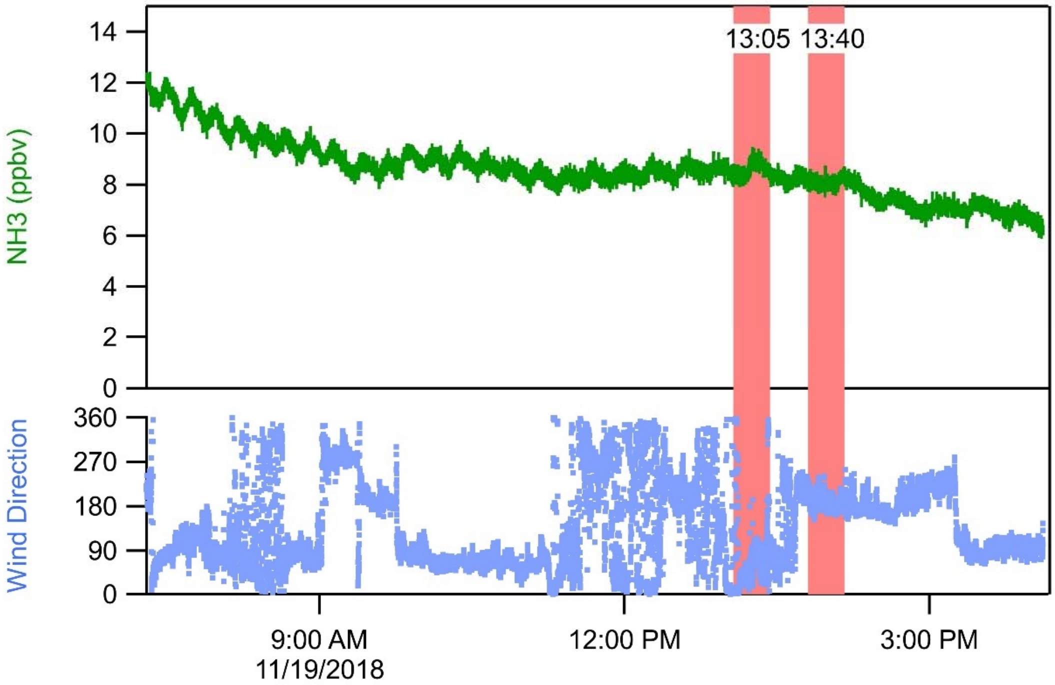

Figure 5-2. Ammonia and Wind Direction Observed by the Mobile Laboratory on November 19, 2018.

The wind direction during both November 19, 2018, ammonia releases is shown in Figure 5-3. The ML was positioned to the south of the farm for the 13:05 releases (Figure 5-1, Location A). The AP Stack was in the north-northeast direction (~15º) in relation to the ML. The dominant wind direction was from the northeast; therefore, the ML was positioned appropriately downwind during the release window. However, even with the correct positioning, the release of a low level of ammonia at 0.6 ppmv within the stack likely means the downwind concentration will be diluted to negligible levels. This makes the 13:40 release of 0.1 ppmv ammonia even less likely to be observed. In addition, the winds were highly variable this day and the ML was not positioned well downwind for the 13:40 release. It was located at Location B in Figure 5-1 with the stack in the north-northwest direction (~340º), but Figure 5-3 shows the wind during this time from the south.

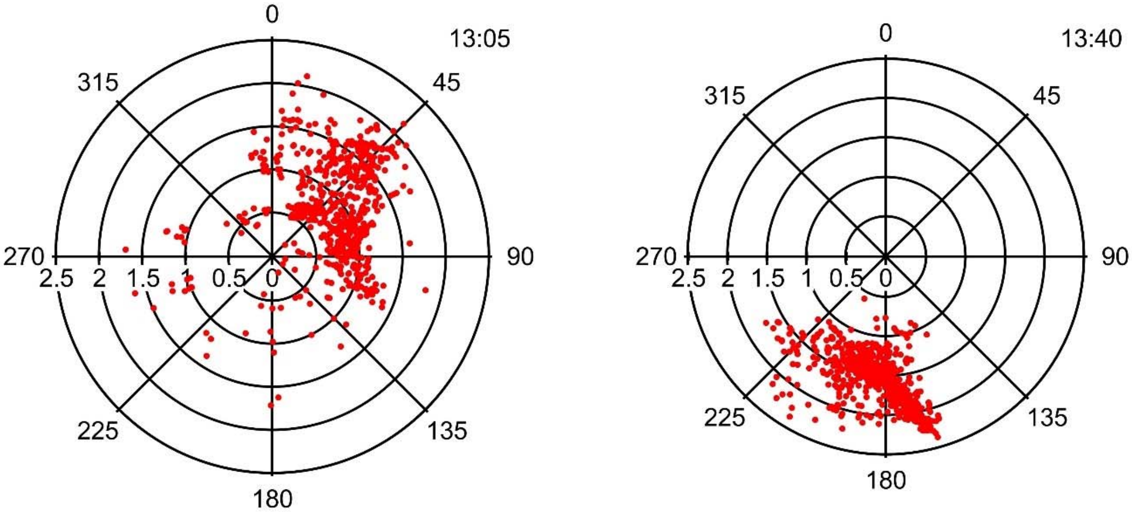

Figure 5-3. Wind Direction During the 13:05 and 13:40 Ammonia Releases on November 19, 2018.

The releases on November 20, 2018, were more frequent and at higher concentrations which provides better opportunities for downwind observation. For all the releases, the ML was at Location B in Figure 5-1 with the AP Stack to the north-northeast (~340°). Figure 5-4 shows the ammonia concentration and wind direction for the entire monitoring period on November 20, 2018, along with the red bars representing the ammonia release periods. The ML did not observe any ammonia increases and the concentrations were representative of typical background levels.

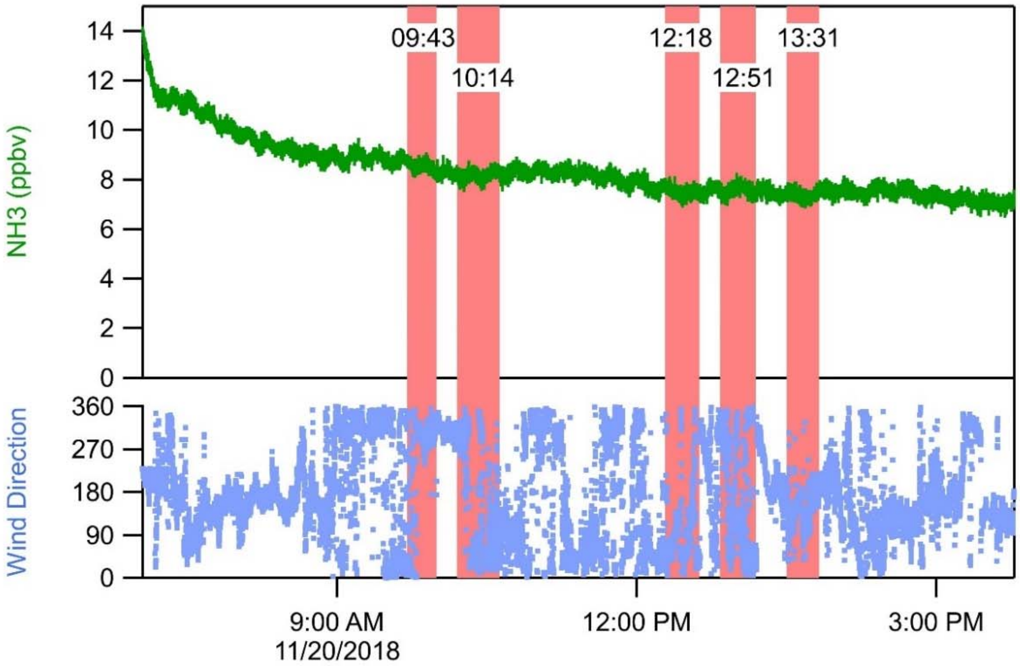

Figure 5-4. Ammonia and Wind Direction Observed by the Mobile Laboratory on November 20, 2018.

The wind was highly variable on November 20, 2018, which makes appropriate positioning of the ML difficult. During the first two ammonia releases at 09:43 and 10:14, a large portion of the wind was from the northeast direction. The 09:43 release was only 1 ppmv; therefore, similar to the November 19, 2018, releases, it is likely diluted to concentrations low enough to be negligible even if the ML was monitoring within the plume. The 10:14 release was the highest at 638 ppmv. Assuming it was injected into the stack at 1 slpm and diluted by a flowing stream of 15 cfm (425 slpm) would mean the ammonia concentration at the output of the stack is 1.5 ppmv. If the stack plume was diluted by a factor of 100 as it traveled downwind the ML could potentially see a 0.015 ppmv response. The ML did not observe any change during this release. One explanation could be that the ML was too close to the stack and the plume traveled above the ML. During the third release of 330 ppmv at 12:18, the wind was not favorable coming predominately from the northeast (Figure 5-5) and no ammonia response was observed. The fourth release of 102 ppmv at 12:51 had winds from the direction of the stack, but like the 10:14 release, no response in ammonia was observed. The fifth release of 0.346 ppmv at 13:31 had the most unfavorable winds with the prevailing wind from the southeast and no response in ammonia was observed. However, given the low concentration of the fifth release, the response after dilution is expected to be negligible.

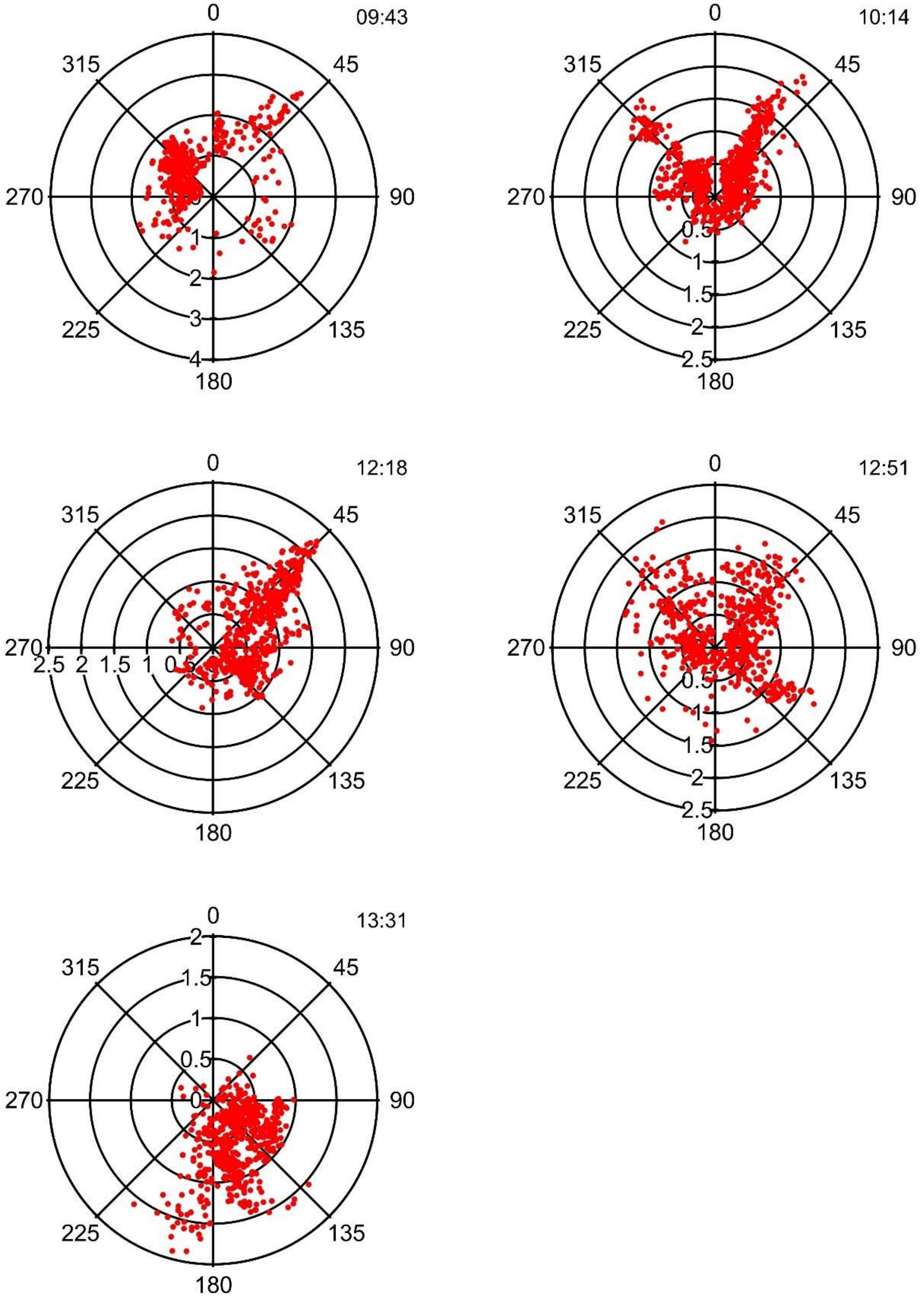

Figure 5-5. Wind Direction During the 09:43, 10:14, 12:18, 12:51, and 13:31 Ammonia Releases on November 20, 2018.

5.3 Septic Analysis

5.4 Discussion of Test Activities and Observations – Septic

One day was spent characterizing and tracking the septic tanks located east of the 242A Evaporator. Table 5-3 Lists the various activities conducted during Septic Tank Monitoring that occurred in Month 4.

Table 5-3. 200 East Septic Analysis.

Week	Date	Description	Activities/Observations
17	11/28/2018	Side Port Monitoring	Septic tanks near 242A Evaporator

Source: Esri, DigitalGlobe, GeoEye, Earthst IGN, and the GIS User Community

Figure 5-6. 200 East Septic Analysis.

5.5 Identification of Vapor Sources and Quantitative Analysis of Vapor Composition – Septic

5.5.1 Septic Composition Response from Literature

Previous work has provided insight into the response of organosulfur compounds (OSCs) within a PTR-TOF-MS (Perraud, 2016). They operated the PTR-TOF-MS in the 130 to 133 Td range, which is slightly higher than the typical 120 Td operation of the PTR-TOF-MS in the ML. This means that there would be more fragmentation reported in Perraud, 2016 compared to the ML observations, but the key ions will remain the same. The species analyzed in the report were methanethiol, dimethyl sulfide, dimethyl disulfide, and dimethyl trisulfide. All these species are suspected of being within the septic emissions. Figure 5-7 was developed using the intensity reported in Table 1 by Perraud, 2016. Methyl mercaptan (reported as methanethiol in Perraud, 2016) shows a strong signal at the MW+1 ion m/z 49. Dimethyl sulfide has a strong response at the MW+1 ion m/z 63. The ML has observed the same strong response while monitoring the dimethyl sulfide within the ML VOC standard. Dimethyl disulfide responds 70% at the MW+1 ion m/z 95, 27% at m/z 79, and 3% at m/z 49. The structure of dimethyl disulfide lends to m/z 79 being an CH_3S_2 fragment. The m/z 49 would have a CH_4S composition (same as methyl mercaptan), but not sure the mechanism that forms this fragment.

Dimethyl trisulfide fragments the most with only 10% of the signal at the MW+1 ion m/z 127. The dominant signal is at m/z 79 (45%) with strong signals at m/z 93, m/z 81, m/z 61, m/z 49, and m/z 45. The possible fragment compositions are $C_2H_5S_2$ (m/z 93), CH_5S_2 (m/z 81), CH_3S_2 (m/z 79), C_2H_5S (m/z 61), CH_4S (m/z 49), and CHS (m/z 45). These are theoretical fragment compositions and the mechanisms to form these compositions are unknown. This analysis covered a small subset of OSC compounds, but it is hypothesized that other OSCs have potential to respond at any of the ions presented in Figure 5-7.

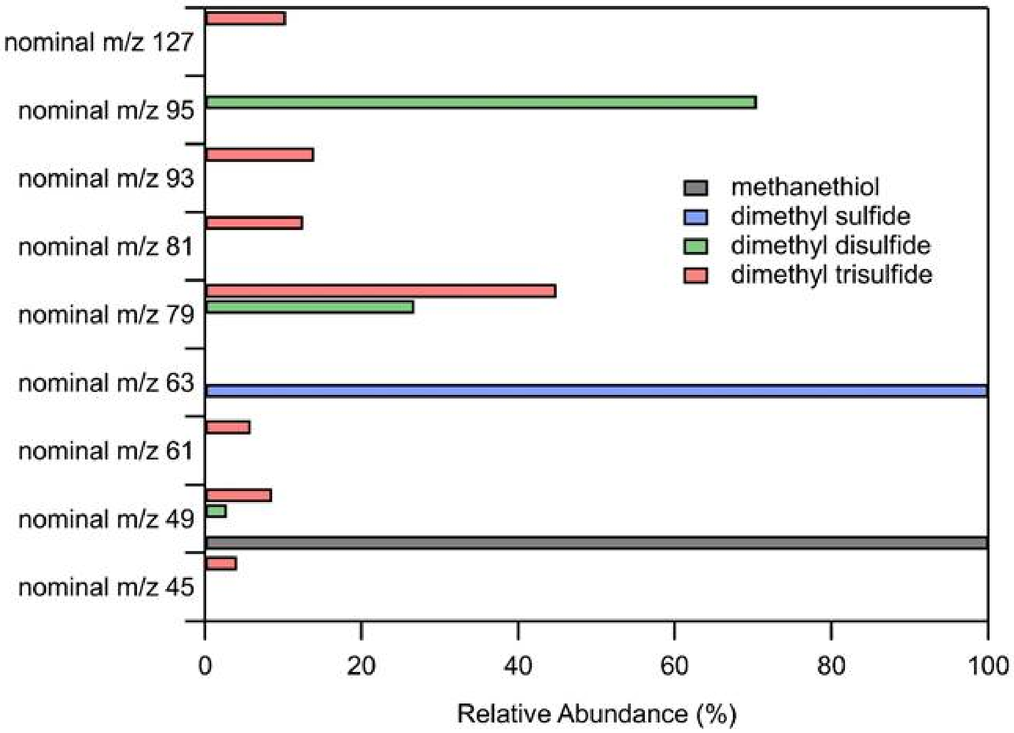

Figure 5-7. Response of Methanethiol (Methyl Mercaptan), Dimethyl Sulfide, Dimethyl Disulfide, and Dimethyl Trisulfide by a PTR-TOF-MS Reported in Perraud, 2016.

5.5.2 Septic Fingerprint November 28, 2018

On November 28, 2018, the ML deployed to monitor emissions from the septic tanks located near the 242-A Evaporator. The 35’ side-port sample line was connected at 07:24. At 07:42, Industrial Hygiene (IH) Technicians connected an SO_2 monitor (MultiRAE®[8] Pro, S/N #MCB3Z008R1) with the assistance of the Subject Matter Expert (SME). No hits of SO_2 were detected during the septic monitoring for this day. The ML Operators moved the inlet incrementally closer to the septic tank throughout the day. Around 10:25, the inlet was moved to above the open septic tank and eventually the lid was placed back on with the inlet inside. Figure 5-8 show a time series of methyl mercaptan, a large constituent of the septic emissions, and ammonia throughout the day. No increase in ammonia was observed within the septic emissions during this monitoring. An average of the septic emissions starting at 11:30, 11:36, and 11:50 were used for fingerprint analysis of the septic emissions.

---

[8] MultiRAE is a registered trademark of RAE Systems, Inc., San Jose, California.

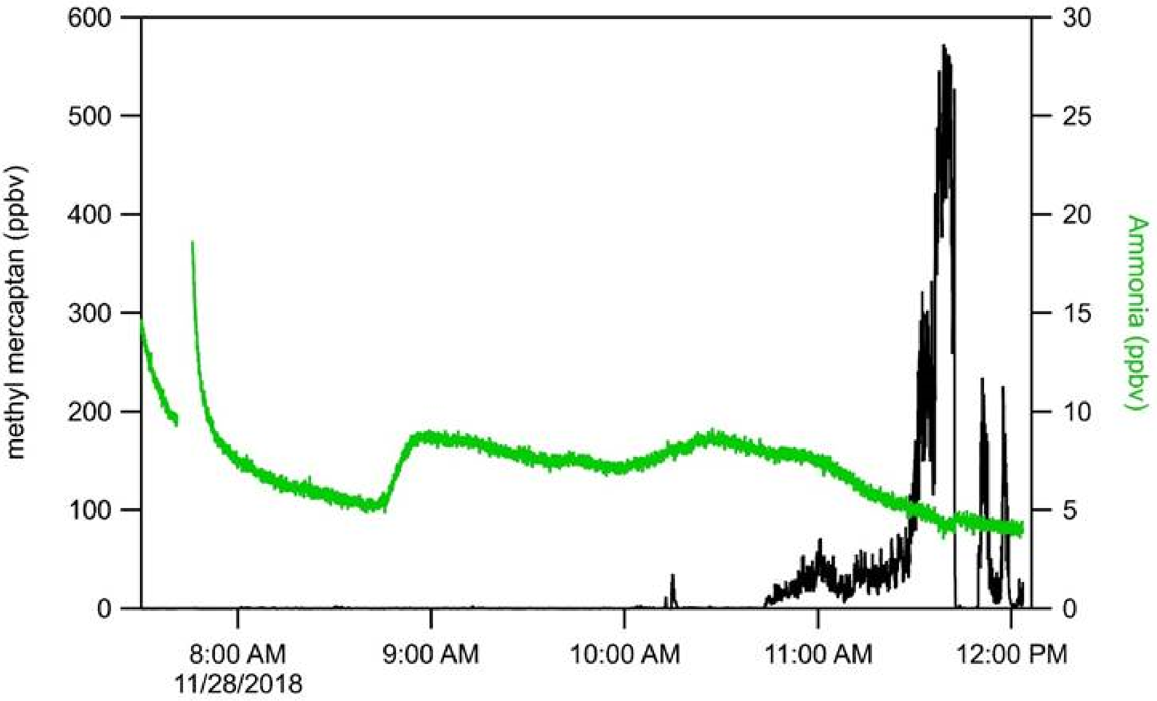

Figure 5-8. Time-series of Methyl Mercaptan and Ammonia During Septic Monitoring on November 28, 2018.

Fingerprint analysis was conducted using the same parameters as the fingerprint analysis from 53005-81-RPT-027, *PTR-MS Mobile Laboratory Vapor Monitoring Monthly Report – Month 2*. To be included in the fingerprint, a species must have a concentration of at least 0.05 ppbv and contribute at least 0.5% to the total abundance of the plume. Figure 5-9 shows the resulting fingerprint for the 11:30, 11:36, and 11:50 plumes. The septic fingerprint from 53005-81-RPT-027 is included for reference. As expected, the composition of the November 28, 2019, plumes are comparable to the Month 2 results. Methyl mercaptan and m/z 35 are the dominant signals with a small contribution at nominal m/z 93. The nominal m/z 35 could potentially be attributed to dihydrogen sulfide (H_2S), which has a molecular weight (MW) of 34 and responds at m/z 35. The OSC fragments identified above are also labeled in Figure 5-9. All the fragments are present within the septic emission fingerprint from Month 2 except m/z 95 and m/z 127, which suggests that dimethyl disulfide and dimethyl trisulfide are either not present or in such low abundance that their response is negligible. Only m/z 93 and m/z 63 (dimethyl sulfide) show up in the November 28, 2019, results with the $C_2H_5S_2$ m/z 93 fragment being attributed to an unidentified OSC. It is possible that differences in the sampling setup with the Month 2 data originated from downwind sampling through the ML mast versus the November 28, 2019, data from the side-port. In addition, the variability in septic system usage and changes in the weather could contribute to changes in septic emission composition. Each experiment advances the knowledge of the septic composition and further studies are recommended.

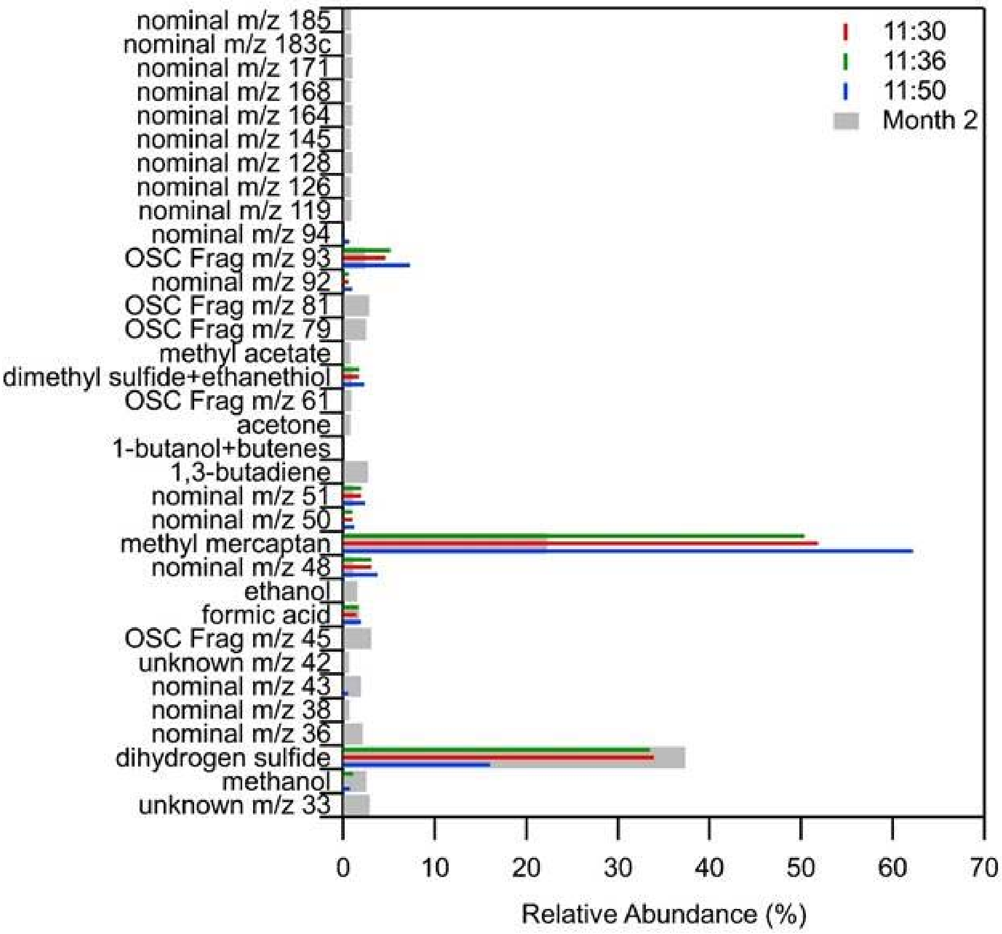

Figure 5-9. Septic Fingerprint of the Plumes Occurring at 11:30, 11:36, and 11:50 on November 28, 2018, along with the Average Septic Plume Developed in Month 2.

5.6 NO^+ Testing

For 5 days of Month 4, the focus was on Selective Reagent Ionization – Mass Spectrometer (SRI-MS) testing of the NO^+ and H_3O^+ modes on the PTR-MS. SRI-MS is a new technology where different reagent ions for chemical ionization direct injection mass spectrometry can be selected. NO^+ mode enables the ability to separate many isomeric compounds and allow for detection and quantification of these compounds. The ML Operators performed numerous tests for switching between NO^+ and H_3O^+ mode, both manually and through automation.

Multipoint calibrations in H_3O^+ and NO^+ mode were performed using the multi-VOC standard cylinder (ID: 160-401265983-1). A multipoint calibration consists of a 10-minute zero followed by four different span levels at 10 minutes each and ends with a second 10-minute zero. The zero-air flow remains constant throughout the calibration and the VOC flow is varied to achieve the four span levels. Figure 5-10 shows a time-series of benzene in NO^+ mode during one of the multipoint calibrations. One multipoint calibration was performed in H_3O^+ mode and two were performed in NO^+ mode.

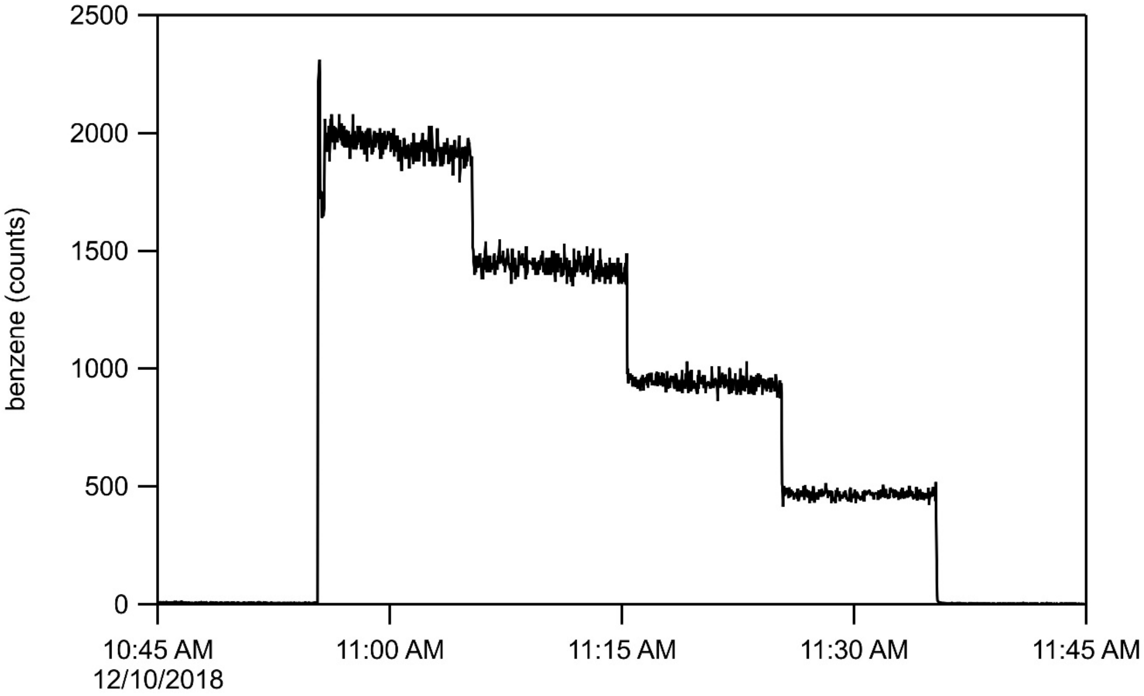

Figure 5-10. Time-series of Benzene Response at m/z 78 During a Multipoint Calibration in NO$^+$ Mode.

There is not always literature available detailing the response of an analyte within the PTR-MS. Furthermore, the values present in the literature may have been obtained under very different conditions such as pressure, temperature, and electric field strength. Therefore, generating known concentrations and monitoring them with the PTR-MS allows identification of the important ions representing an individual analyte. Figure 5-11 shows the mass spectra for benzene for H_3O^+ and NO$^+$ modes. The molecular weight of benzene is 78 and the reaction with H_3O^+ generates a signal at m/z 79 due to the addition of a proton. There is also a noticeable peak at m/z 80, which can be attributed to the presence of a C^{13} isotope within the species. The isotopic abundance of C^{13} compared to C^{12} is ~1.11%. Since there are six carbons in benzene, it has a 6 x 1.11% to equal a 6.66% chance of one of them being C^{13}. The red trace for H_3O^+ in Figure 5-11 shows a maximum of ~171 counts at m/z 79 and a maximum of ~11 counts at m/z 80. The signal at m/z 80 is approximately 6.43% of the m/z 79 signal, which is very close to the expected 6.66%.

Looking at the NO$^+$ portion of Figure 5-11, a mass shift in the response is observed reflecting the different ionization mechanism at work. This charge transfer reaction with NO$^+$ produces an ion at the molecular weight of benzene, m/z 78. As observed for the H_3O^+ response, there is a response at m/z 79 in NO$^+$ mode attributed to the presence of C^{13}. Looking at the read trace for NO$^+$ in Figure 5-11, the signal at m/z 79 is approximately 7.6% the signal at m/z 78. This is slightly higher than the expected 6.6% but is close enough that the signal is still likely attributed to the presence of C^{13}. Data processing to convert the raw signal (counts) into a concentration (ppbv) utilizes the dominant ion signal (m/z 79 for H_3O^+, m/z 78 for NO$^+$) and does not include the response generated from isotopes of any elements.

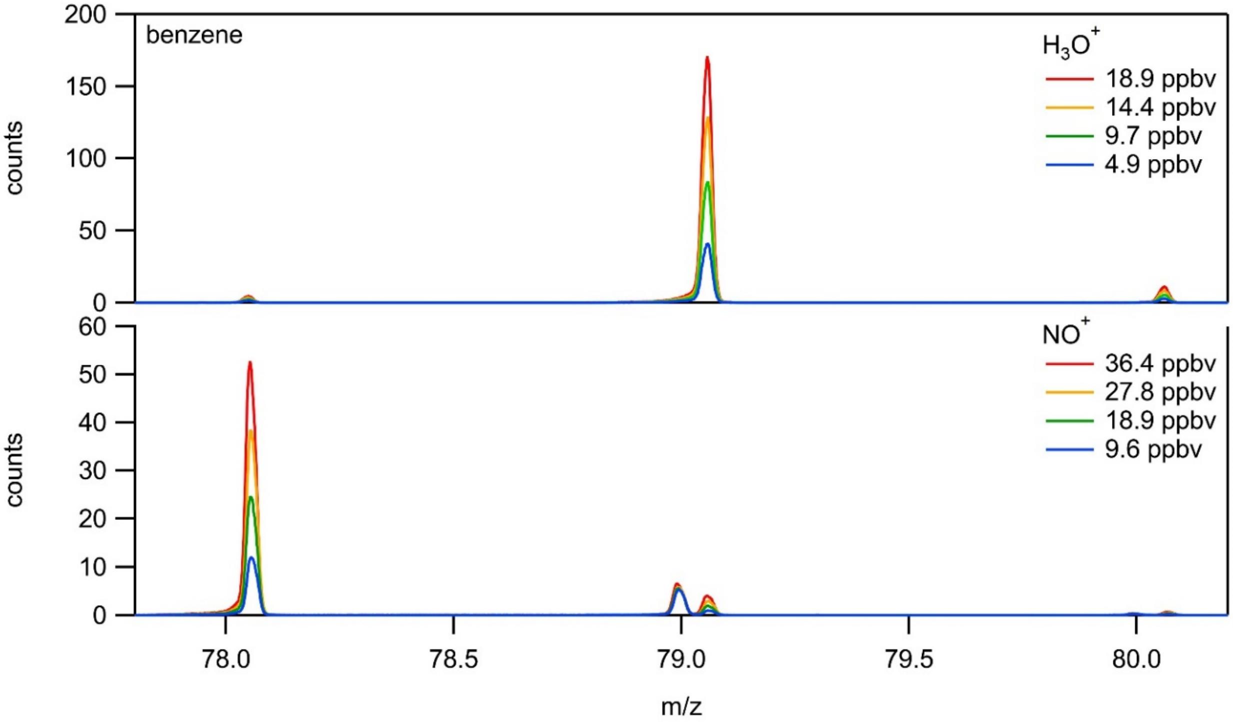

Figure 5-11. Mass Spectra of Benzene Peaks Observed in H_3O^+ and NO^+ Modes.

Quantification using the PTR-MS requires knowledge of the kinetics involved in the reactions and the behavior of the ions within the instrument. While using theoretical calculations based on the understood kinetics may result in accurate quantification, there are often unknown or difficult-to-quantify effects within the instrument that reduce the confidence in the kinetic calculations. Specifically, the transmission efficiency of the ions traveling from the drift tube to the detector can play a major part in skewing the results. In addition, the kinetics of all species are not known; therefore, estimations and assumptions must be made, which reduce confidence once again. Calibrations also provide a valuable check on possible changes of parameters in this particular PTR-MS and can be a valuable diagnostic for troubleshooting if necessary.

The multipoint calibrations allow for a metric to empirically estimate the kinetics and transmission efficiency at the same time. Sampling a known concentration of an analyte allow for characterization of its behavior for the entire process. The process is as follows.

1. Conduct multipoint calibration(s) at a reasonable dynamic range relevant to the target concentrations.

2. Process the data and produce a response without applying kinetics and transmission efficiency.

3. Compare the processed results to the expected concentrations generated by the calibration system. Use the correlation between the expected concentration and the observed signal to get a sensitivity.

These steps were performed for 18 species that were available in a gas standard at the time. Each of the four levels of the multipoint calibration were compared to the expected result from the calibration system. The expected results are calculated using the following equation:

$$[expected, ppbv] = [tank\ concentation, ppbv] * \frac{[calibration\ flow, sccm]}{(\ [calibration\ flow, sccm] + [zero\ flow, sccm]\ )}$$

Figure 5-12 shows the resulting correlation between the observed benzene signal and expected benzene concentrations for the December 10, 2018, multipoint calibration. There was a good correlation with an r^2 of 0.999, which gives confidence in the ability to produce and monitor desired concentrations with the calibration system. The slope is representative of the sensitivity of benzene and is reported as 54.431 counts per ppbv. This calibration factor empirically estimates kinetics, transmission efficiency, and any other factor within the instrument that can affect the ability to quantify an analyte. This factor can be used to correct the observed response and account for the lack of knowledge concerning the kinetics, transmission efficiency, and other factors. These calibration factors were developed for the analytes that can be confidently generated as known concentrations using the calibration system and available standards.

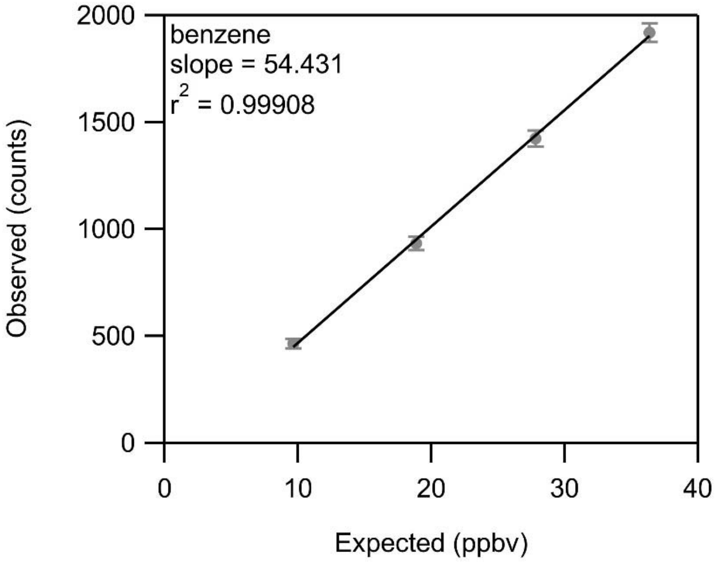

Figure 5-12. Correlation Between the Observed and Expected Benzene Concentrations.

To process the raw signal into a concentration the following formula is used:

$$[analyte, ppbv] = \frac{([raw\ signal, counts] - [instrument\ baseline, counts])}{\left[calibration\ factor, \frac{counts}{ppbv}\right]}$$

The raw signal and instrument baseline are the normalized signals produced from the PTR-MS data processing software. The instrument baseline is the average of the signal when the PTR-MS is sampling gas from an ultra-zero-air cylinder. Looking back at Figure 5-10, the PTR-MS was sampling zero-air from 10:45 to 10:55 then again from 11:35 to 11:45. Figure 5-13 shows the benzene raw signal for the first zero. Taking the average from 10:45 to 10:55 gives the instrument baseline represented by the red line, which is 6.93 counts. Since air that does not contain benzene is being sampled, this is representative of the response in the instrument when there is no benzene. Therefore, it is important to subtract this baseline signal for all the benzene data. The blue trace in Figure 5-13 is the raw signal minus the instrument baseline and the signal now hovers around zero.

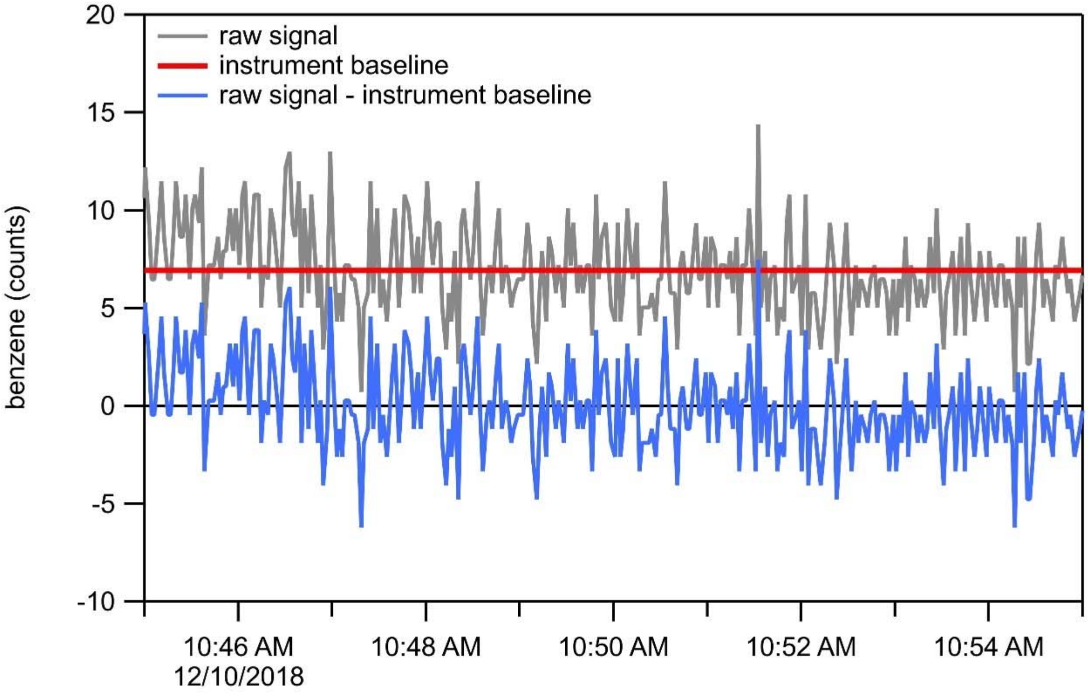

Figure 5-13. Time-series of Benzene While Sampling Zero-air Coupled with the Resulting Time Series after Subtracting Instrument Baseline.

The instrument baseline and calibration factor can now be input into the equation to calculate the concentration of benzene for any given raw data point.

$$[benzene, ppbv] = \frac{([benzene\ raw\ signal, counts] - [6.93\ counts])}{\left[54.431\ \frac{counts}{ppbv}\right]}$$

Figure 5-14 shows the benzene raw signal along with the average signal during one of the calibration levels equal approximately 1436 counts. Inserting this value into the above equation results in a benzene concentration of 26.3 ppbv of benzene. For this calibration level, the zero flow was 1000 sccm, calibration flow was 60 sccm, and the concentration of benzene in the calibration tank is 491 ppbv. Using the equation for calculating expected concentration detailed above, this results in an expected concentration of benzene to be 27.8 ppbv. This calculated concentration is approximately 5.5% different than the expected. The accuracy of the VOCs in the standard is ±20% and a difference within these bounds is acceptable.

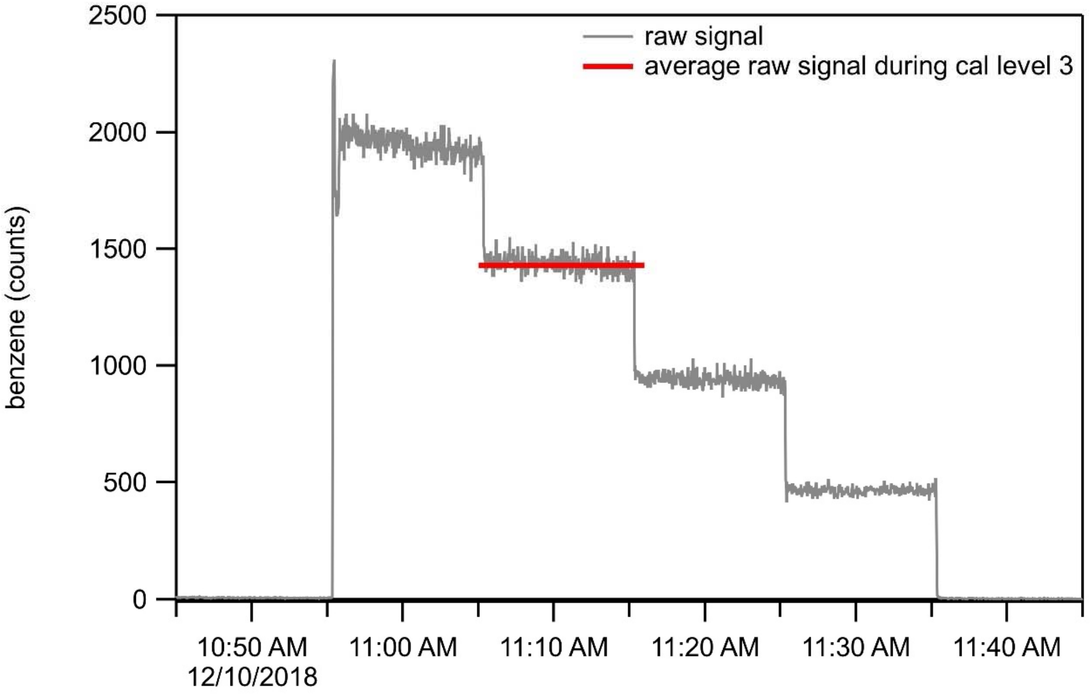

Figure 5-14. Time Series of Benzene Response at m/z 78 During a Multi-point Calibration in NO^+ Mode.

It is important to note that these sensitivities are not static. While the reaction kinetics will remain the same, changes in instrument performance and transmission efficiency will affect the sensitivities. Therefore, it is important to perform periodic spans and multipoint calibrations to capture the current sensitivities. This process was repeated for the remaining selection of VOCs and presented below. Multipoint calibrations occurring on December 6, 2018; December 7, 2018; and December 10, 2018, were used in the following analysis. It is also important to note that the ionization potential (IP) of NO is 9.26 eV; thus ionization is energetically forbidden for compounds having an IP > 9.26 eV. This includes target compounds in for Month 4 which are incorporated for completeness and labeled as "NO^+" for consistency, although it is probable that ionization in those cases proceeds by charge transfer to O_2^+ with an IP of 12.07 eV. It is also noted that three mechanisms are available for ionization by NO+, charge transfer, hydride, abstraction, and clustering (adduct formation). The preferred mechanism depends primarily on the difference in the IP though other factors may be at play. Only the charge transfer products are reported here, and investigation of the other ionization channels is left as a possibility for future work.

5.6.1 Methanol (m/z 32)

Figure 5-15 shows the mass spectra of methanol during H_3O^+ and NO^+ modes. In H_3O^+ mode, the response is at m/z 33, which is the MW+1 ion as expected. The IP of methanol is 10.84 eV. Comparing this to the IP of NO at 9.26 eV, methanol will not undergo a charge transfer with NO meaning there will be no response. The large signal at m/z 32 is due to O_2^+. Production of NO^+ in the ion source uses O_2 and N_2 gas. A byproduct of the production is formation of O_2^+ ions. The ion source is tuned to limit the amount of O_2^+ production, but an O_2^+ signal up to a magnitude of 4% of the NO^+ signal can be present. Since NO^+ will be present on the order of 10^7 power, there will be a substantial O_2^+ signal on the order of 10^5. Given this, quantification of methanol in NO^+ mode is not reliable, and no sensitivity will be reported.

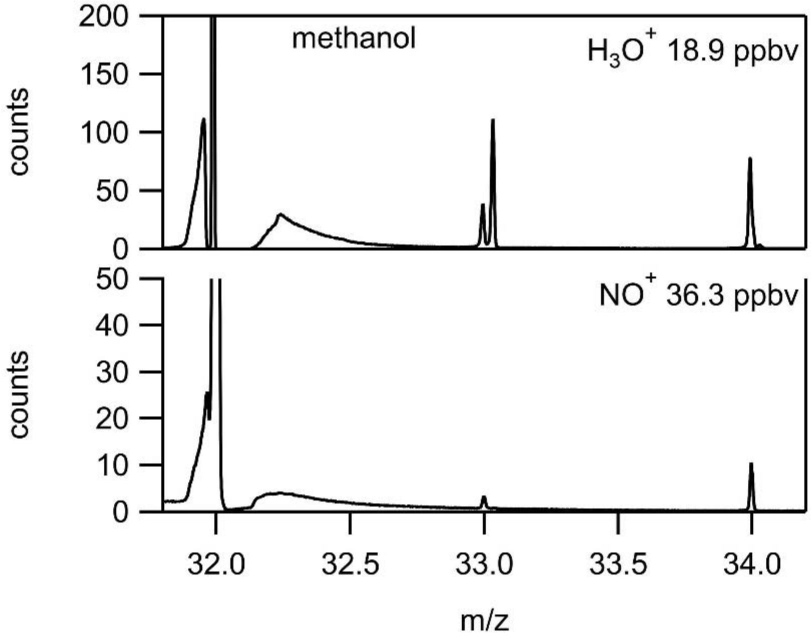

Figure 5-15. Mass Spectra of Methanol Response During H_3O^+ and NO^+ Modes.

5.6.2 Acetonitrile (m/z 41)

Figure 5-16 shows the mass spectra of acetonitrile during H_3O^+ and NO^+ modes. In H_3O^+ mode the response is at m/z 42, which is the MW+1 ion as expected, and at m/z 41 in NO^+ mode. The IP of acetonitrile is 12.20 eV. Comparing this to the IP of NO at 9.26 eV, acetonitrile will not undergo a charge transfer with NO meaning that the m/z 41 response is not due to a reaction with NO^+. It is likely a reaction with O_2^+ (IP = 12.07) producing a response at m/z 41. Even though the ion source is tuned to produce NO^+, it is difficult to not produce low levels of O_2^+ and H_3O^+ in the process. The ion source is tuned to limit the quantity of O_2^+ and H_3O^+ during NO^+ mode. Given this, quantification of acetonitrile in NO^+ mode is not reliable, and no sensitivity will be reported.

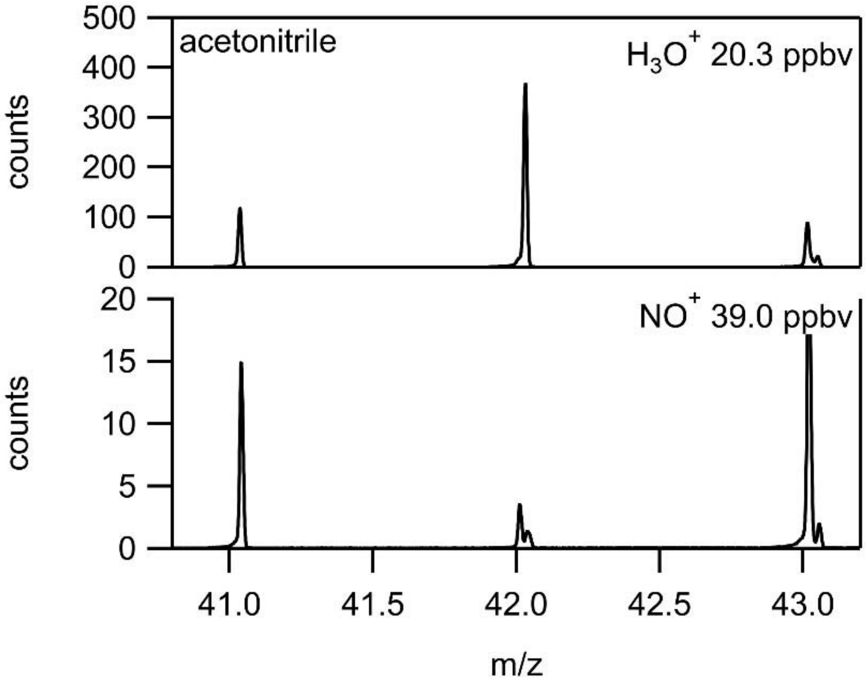

Figure 5-16. Mass Spectra of Acetonitrile Response During H_3O^+ and NO^+ Modes.

5.6.3 Acetaldehyde (m/z 44)

Figure 5-17 shows the mass spectra of acetaldehyde during H_3O^+ and NO^+ modes. In H_3O^+ mode, the response is at m/z 45, which is the MW+1 ion as expected. In NO^+ mode, the largest response remains at m/z 45 with a smaller response at m/z 44. The IP of acetaldehyde is 10.229 eV. Comparing this to the IP of NO at 9.26 eV, acetaldehyde will not undergo a charge transfer with NO meaning that the m/z 44 response is not due to a reaction with NO^+. It is likely a reaction with O_2^+ (IP = 12.07) producing a response at m/z 44 and reaction with H_3O^+ is producing a response at m/z 45. Even though the ion source is tuned to produce NO^+, it is difficult to not produce low levels of O_2^+ and H_3O^+ in the process. The ion source is tuned to limit the quantity of O_2^+ and H_3O^+ during NO^+ mode. Given this, quantification of acetaldehyde in NO^+ mode is not reliable, and no sensitivity will be reported.

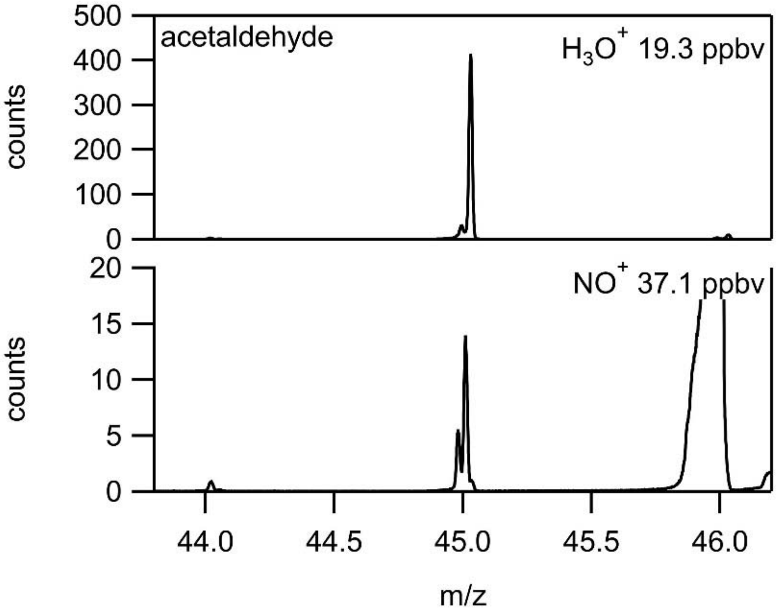

Figure 5-17. Mass Spectra of Acetaldehyde Response During H_3O^+ and NO^+ Modes.

5.6.4 1,3-butadiene (m/z 54)

Figure 5-18 shows the mass spectra of 1,3-butadiene during NO^+ modes. The 1,3-butadiene was not run in H_3O^+ mode and responds at m/z 54 in NO^+ mode. The IP of 1,3-butadiene is 9.07 eV, which is lower than NO (9.26 eV) and makes it a good candidate for NO^+ mode sampling. There are no interferences at m/z 54 and this ion will be used to calculate the sensitivity of 1,3-butadiene.

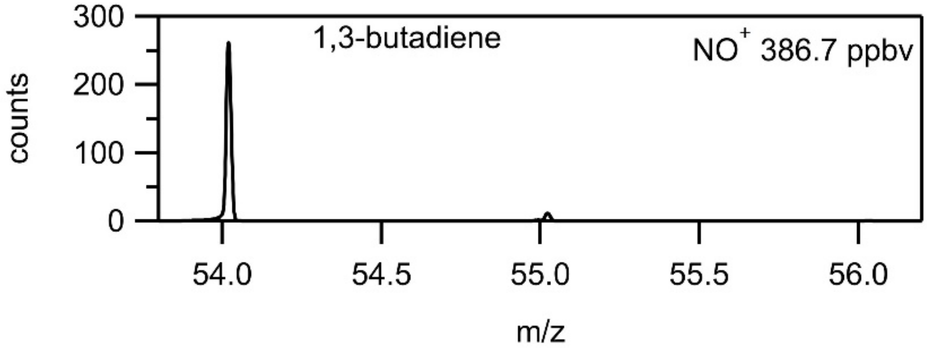

Figure 5-18. Mass Spectra of 1,3-butadiene Response During H_3O^+ and NO^+ Modes.

Figure 5-19 shows the observed counts at m/z 54 during a multipoint calibration versus the calculated expected concentration. The counts shown in Figure 5-19 are a result of calculating the area under the peak shown in Figure 5-18. An r^2 of 0.9995 shows a good fit and the slope of 28.851 counts/ppbv shows that 1,3-butadiene is sensitive enough to allow for a good response in NO^+ mode.

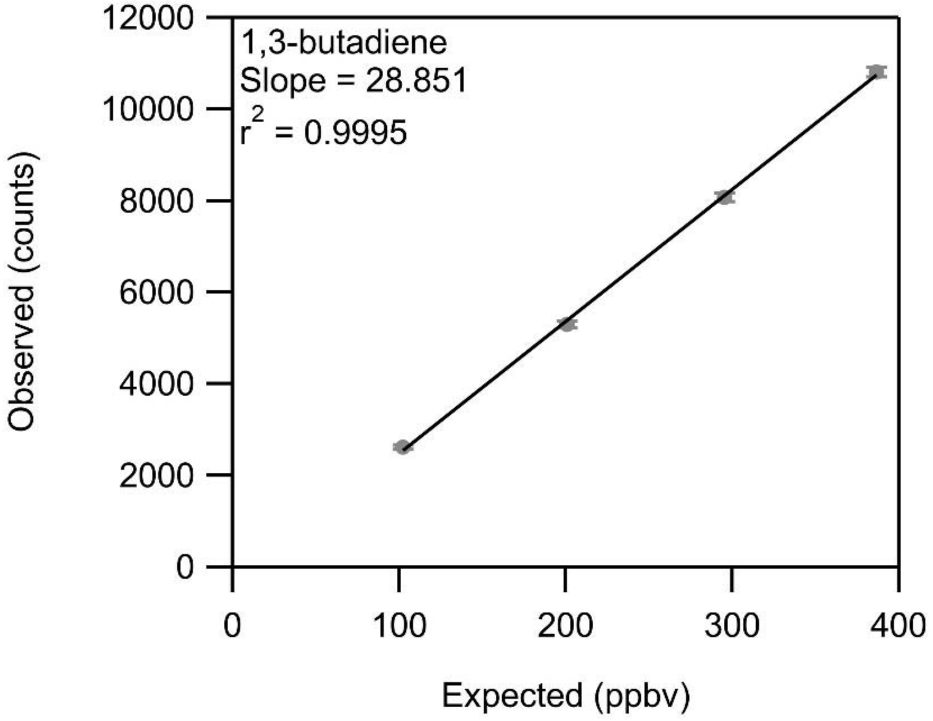

Figure 5-19. Correlation Between the Observed Signal and Expected Concentration of 1,3-butadiene.

5.6.5 1-butene (m/z 56)

Figure 5-20 shows the mass spectra of 1-butene during H_3O^+ and NO^+ modes. In H_3O^+ mode, the response is at m/z 57, which is the MW+1 ion as expected. In NO^+ mode, the largest response remains at m/z 57 with a smaller response at m/z 56. The IP of 1-butene is 9.58 eV. Comparing this to the IP of NO at 9.26 eV, 1-butene will not undergo a charge transfer with NO meaning that the m/z 62 response is not due to a reaction with NO^+. It is likely a reaction with O_2^+ (IP = 12.07) producing a response at m/z 56 and reaction with H_3O^+ is producing a response at m/z 57. Even though the ion source is tuned to produce NO^+, it is difficult to not produce low levels of O_2^+ and H_3O^+ in the process. The ion source is tuned to limit the quantity of O_2^+ and H_3O^+ during NO^+ mode. Given this, quantification of 1-butene in NO^+ mode is not reliable, and no sensitivity will be reported.

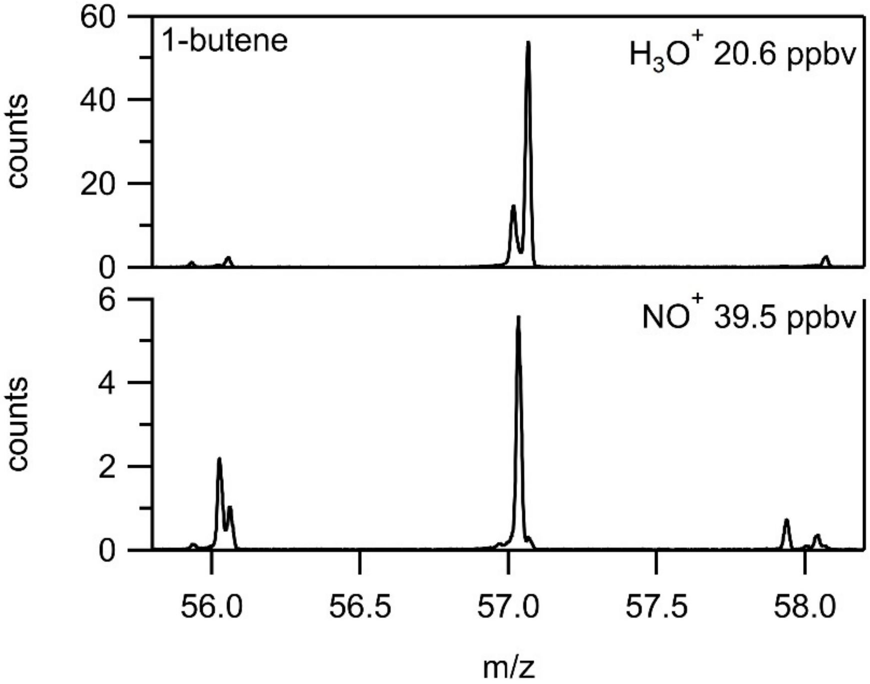

Figure 5-20. Mass Spectra of 1-butene Response During H_3O^+ and NO^+ Modes.

5.6.6 Acetone (m/z 58)

Figure 5-21 shows the mass spectra of acetone during H_3O^+ and NO^+ modes. In H_3O^+ mode, the response is at m/z 59, which is the MW+1 ion as expected. In NO^+ mode, the largest responses occur at m/z 58 and m/z 59. The IP of acetone is 9.7 eV. Comparing this to the IP of NO at 9.26 eV, acetone will not undergo a charge transfer with NO meaning that the responses observed in NO^+ mode are not caused by a reaction with NO^+. It is likely a reaction with O_2^+ (IP = 12.07) producing a response at m/z 56 and reaction with H_3O^+ is producing a response at m/z 57. Even though the ion source is tuned to produce NO^+, it is difficult to not produce low levels of O_2^+ and H_3O^+ in the process. The ion source is tuned to limit the quantity of O_2^+ and H_3O^+ during NO^+ mode. Given this, quantification of acetone in NO^+ mode is not reliable, and no sensitivity will be reported.

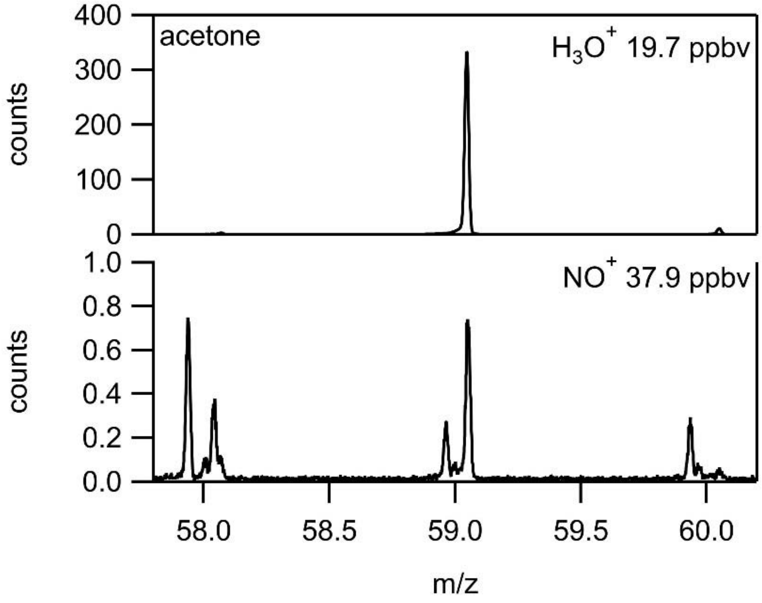

Figure 5-21. Mass Spectra of Acetone Response During H_3O^+ and NO^+ Modes.

5.6.7 Dimethylsulfide (m/z 62)

Figure 5-22 shows the mass spectra of dimethylsulfide during H_3O^+ and NO^+ modes. In H_3O^+ mode, the response is at m/z 63, which is the MW+1 ion as expected, and at m/z 62 in NO^+ mode. The IP of dimethylsulfide is 8.69 eV, which is lower than NO (9.26 eV) and makes it a good candidate for NO^+ mode sampling. There are no interferences at m/z 62 and this ion will be used to calculate the sensitivity of dimethylsulfide.

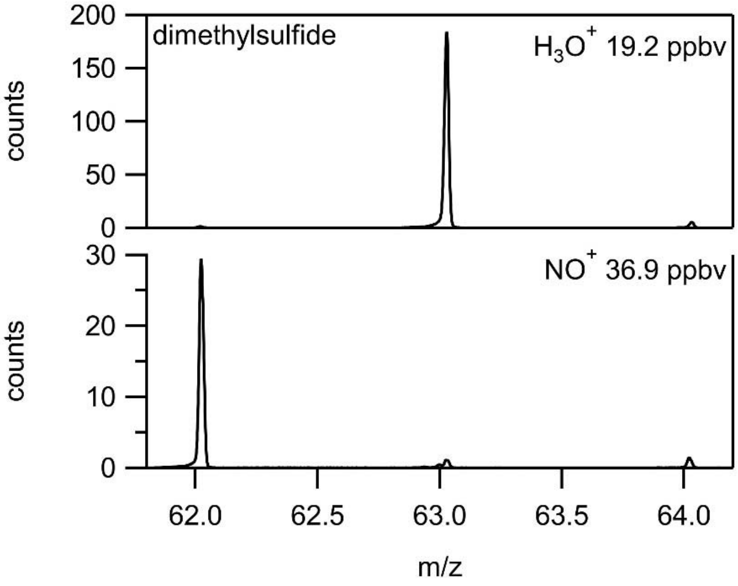

Figure 5-22. Mass Spectra of Dimethylsulfide Response During H_3O^+ and NO^+ Modes.

Figure 5-23 shows the observed counts at m/z 62 during a multipoint calibration versus the calculated expected concentration. The counts shown in Figure 5-23 are a result of calculating the area under the peak shown in Figure 5-22. An r^2 of 0.996 shows a good fit and the slope of 32.524 counts/ppbv shows that dimethylsulfide is sensitive enough to allow for a good response in NO^+ mode.

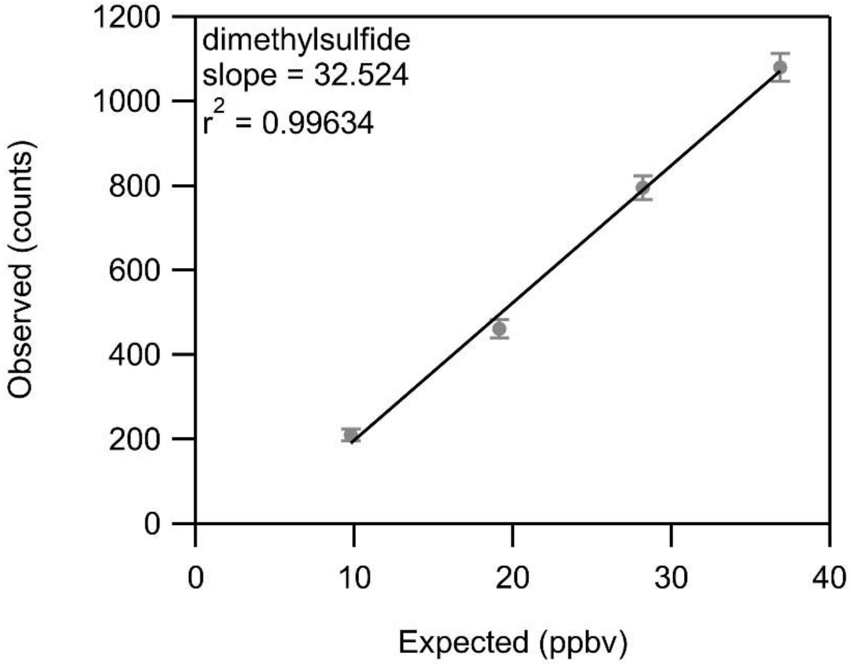

Figure 5-23. Correlation Between the Observed Signal and Expected Concentration Dimethylsulfide.

5.6.8 Furan (m/z 68a)

Figure 5-24 shows the mass spectra of furan during H_3O^+ and NO^+ modes. In H_3O^+ mode, the response is at m/z 69, which is the MW+1 ion as expected, and at m/z 68 in NO^+ mode. The IP of furan is 8.88 eV, which is lower than NO (9.26 eV) and makes it a good candidate for NO^+ mode sampling. The m/z 68 ion will be used to calculate the sensitivity of furan.

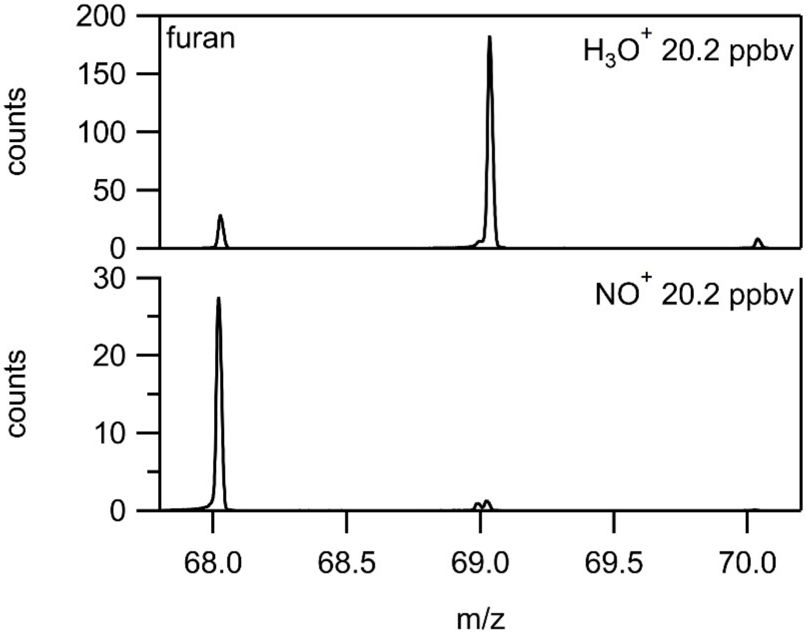

Figure 5-24. Mass Spectra of Furan Response During H_3O^+ and NO^+ Modes.

Figure 5-25 shows the observed counts at m/z 68 during a multipoint calibration versus the calculated expected concentration. The counts shown in Figure 5-25 are a result of calculating the area under the peak shown in Figure 5-24. An r^2 of 0.9996 shows a good fit and the slope of 59.634 counts/ppbv shows that furan is sensitive enough to allow for a good response in NO^+ mode.

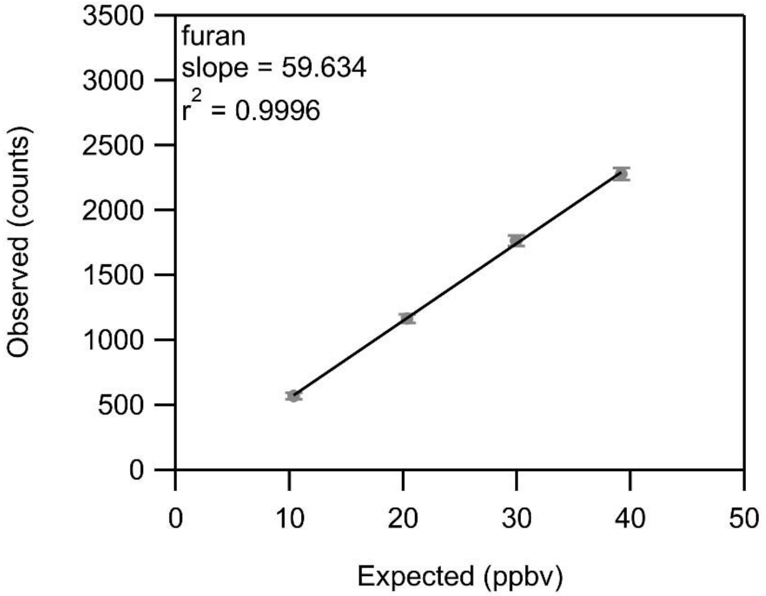

Figure 5-25. Correlation Between the Observed Signal and Expected Concentration of Furan.

5.6.9 Isoprene (m/z 68b)

Figure 5-26 shows the mass spectra of furan and isoprene during H_3O^+ and NO^+ modes. Furan and isoprene are both in the calibration tank used for this testing. In H_3O^++ mode, the response is at m/z 69, which is the MW+1 ion as expected, and at m/z 68 in NO^+ mode. The IP of isoprene is 8.86 eV, which is lower than NO (9.26 eV) and makes it a good candidate for NO^+ mode sampling. There is enough separation between furan and isoprene that there is no interference and the m/z 68 ion will be used to calculate the sensitivity of isoprene.

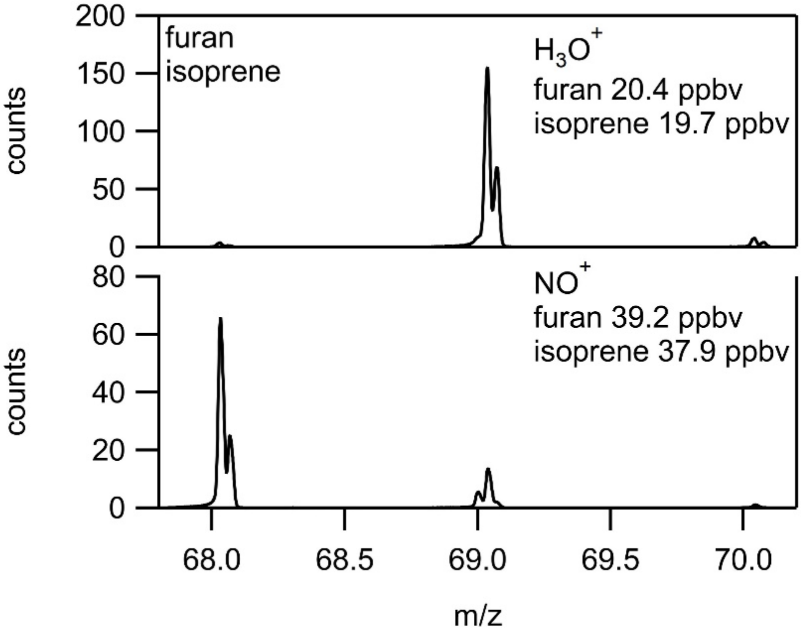

Figure 5-26. Mass Spectra of Furan and Isoprene Response During H_3O^+ and NO^+ Modes.

Figure 5-27 shows the observed counts at m/z 68 during a multipoint calibration versus the calculated expected concentration. The counts shown in Figure 5-27 are a result of calculating the area under the peak shown in Figure 5-26. An r^2 of 0.9999 shows a good fit and the slope of 26.7 counts/ppbv shows that isoprene is sensitive enough to allow for a good response in NO^+ mode.

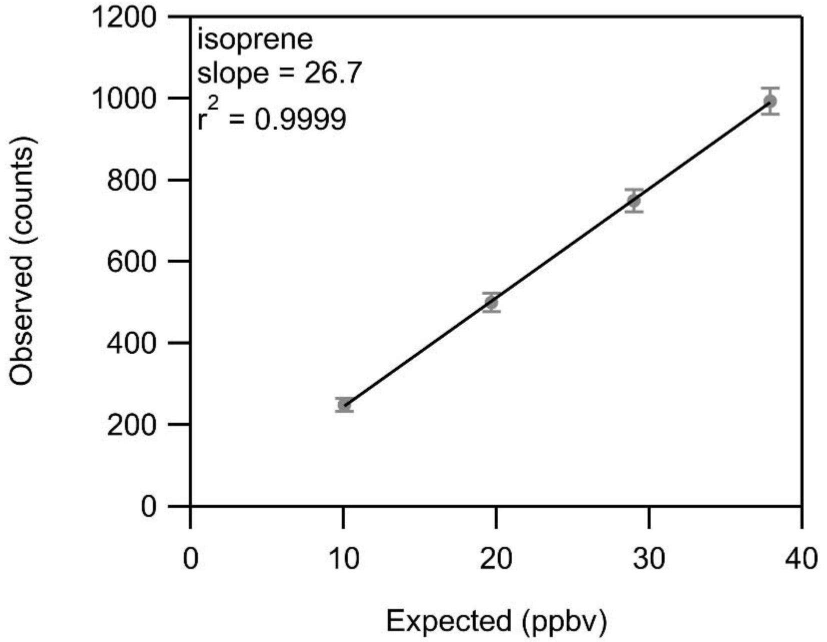

Figure 5-27. Correlation Between the Observed Signal and Expected Concentration of Isoprene.

5.6.10 Methyl Vinyl Ketone + Methacrolein (m/z 70)

Figure 5-28 shows the mass spectra of methyl vinyl ketone and methacrolein during H_3O^+ and NO^+ modes. Methyl vinyl ketone and methacrolein are both in the calibration tank used for this testing. In H_3O^+ mode, the response is at m/z 71, which is the MW+1 ion as expected. In NO^+ mode, the largest response occurs at m/z 71 with a smaller response at m/z 70. The response at m/z 72 is due to the presence of methyl ethyl ketone in the calibration tank used and will be addressed in the next section. The IP of methyl vinyl ketone and methacrolein are 9.65 eV and 9.9 eV, respectively. Comparing this to the IP of NO at 9.26 eV, methyl vinyl ketone and methacrolein will not undergo a charge transfer with NO meaning that the responses observed in NO^+ mode are not caused by a reaction with NO^+. It is likely a reaction with O_2^+ (IP = 12.07) producing a response at m/z 70 and reaction with H_3O^+ is producing a response at m/z 71. Even though the ion source is tuned to produce NO^+, it is difficult to not produce low levels of O_2^+ and H_3O^+ in the process. The ion source is tuned to limit the quantity of O_2^+ and H_3O^+ during NO^+ mode. Given this, quantification of methyl vinyl ketone and methacrolein in NO^+ mode is not reliable, and no sensitivity will be reported.

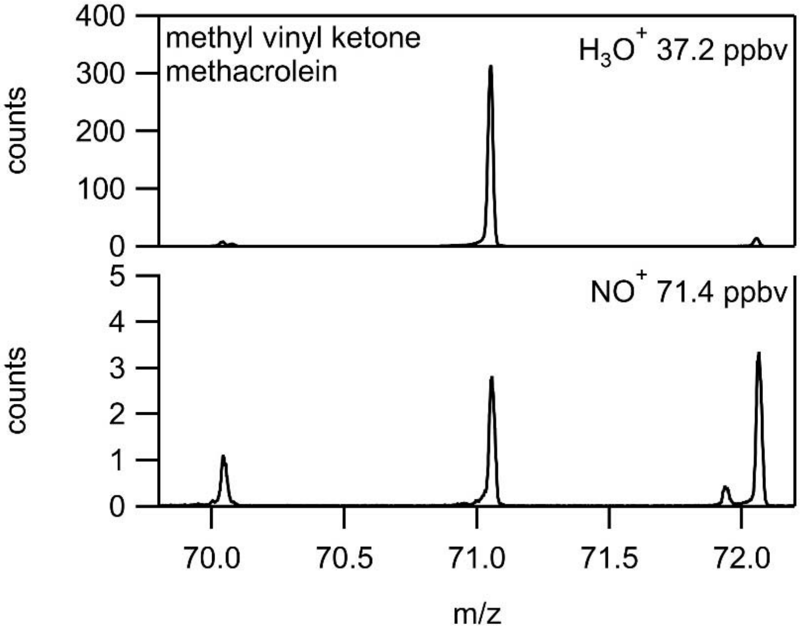

Figure 5-28. Mass Spectra of Methyl Vinyl Ketone and Methacrolein Response During H_3O^+ and NO^+ Modes.

5.6.11 Methyl Ethyl Ketone (m/z 72)

Figure 5-29 shows the mass spectra of methyl ethyl ketone during H_3O^+ and NO^+ modes. In H_3O^+ mode, the response is at m/z 73, which is the MW+1 ion as expected. In NO^+ mode, the largest response occurs at m/z 72 with a smaller response at m/z 73. The IP of methyl ethyl ketone is 9.53 eV. Comparing this to the IP of NO at 9.26 eV, methyl ethyl ketone will not undergo a charge transfer with NO meaning that the responses observed in NO^+ mode are not caused by a reaction with NO^+. It is likely a reaction with O_2^+ (IP = 12.07) producing a response at m/z 72 and reaction with H_3O^+ is producing a response at m/z 73. Even though the ion source is tuned to produce NO^+, it is difficult to not produce low levels of O_2+ and H_3O^+ in the process. The ion source is tuned to limit the quantity of O_2^+ and H_3O^+ during NO^+ mode. Given this, quantification of methyl ethyl ketone in NO^+ mode is not reliable, and no sensitivity will be reported.

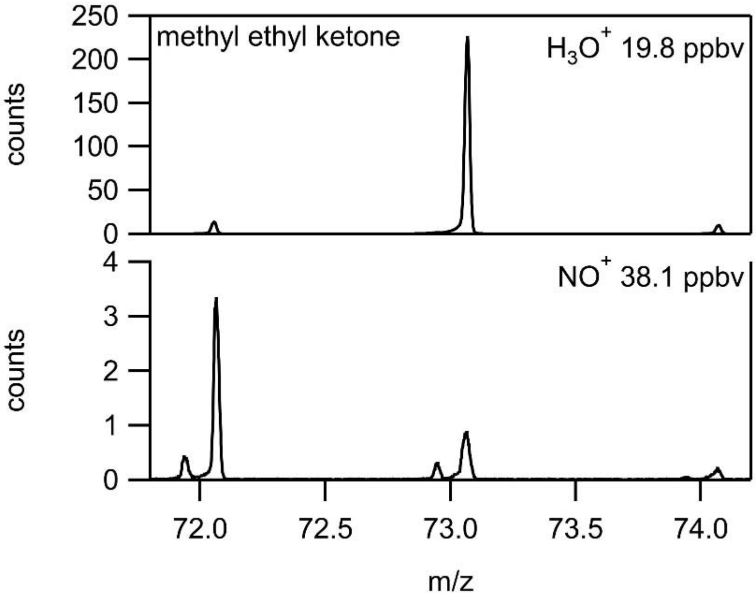

Figure 5-29. Mass Spectra of Methyl Ethyl Ketone Response During H_3O^+ and NO^+ Modes.

5.6.12 NDMA (m/z 74)

Figure 5-30 shows the mass spectra of NDMA during H_3O^+ and NO^+ modes. In H_3O^+ mode, the response is at m/z 75, which is the MW+1 ion as expected, and at m/z 74 in NO^+ mode. The IP of NDMA is 8.69 eV, which is lower than NO (9.26 eV) and makes it a good candidate for NO^+ mode sampling. The m/z 74 ion will be used to calculate the sensitivity of NDMA.

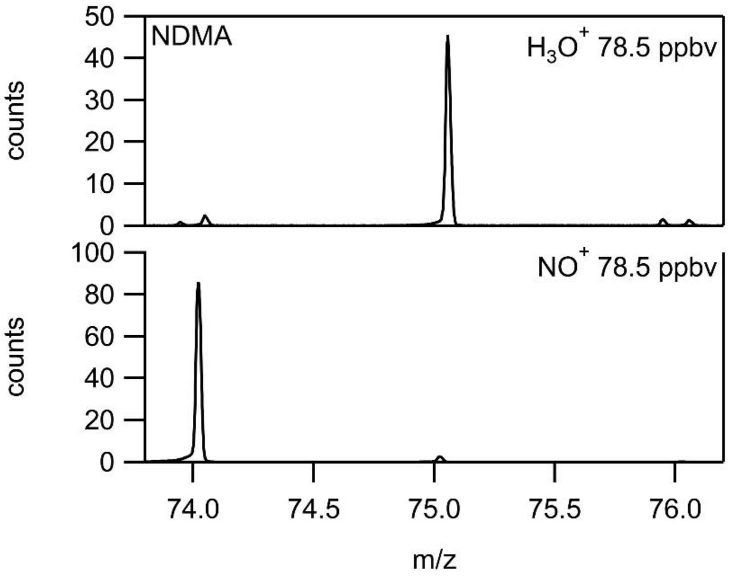

Figure 5-30. Mass Spectra of NDMA Response During H_3O^+ and NO^+ Modes.

Figure 5-31 shows the observed counts at m/z 74 during a multipoint calibration versus the calculated expected concentration. The counts shown in Figure 5-31 are a result of calculating the area under the peak shown in Figure 5-30. An r^2 of 0.9998 shows a good fit and the slope of 41.943 counts/ppbv shows that NDMA is sensitive enough to allow for a good response in NO^+ mode.

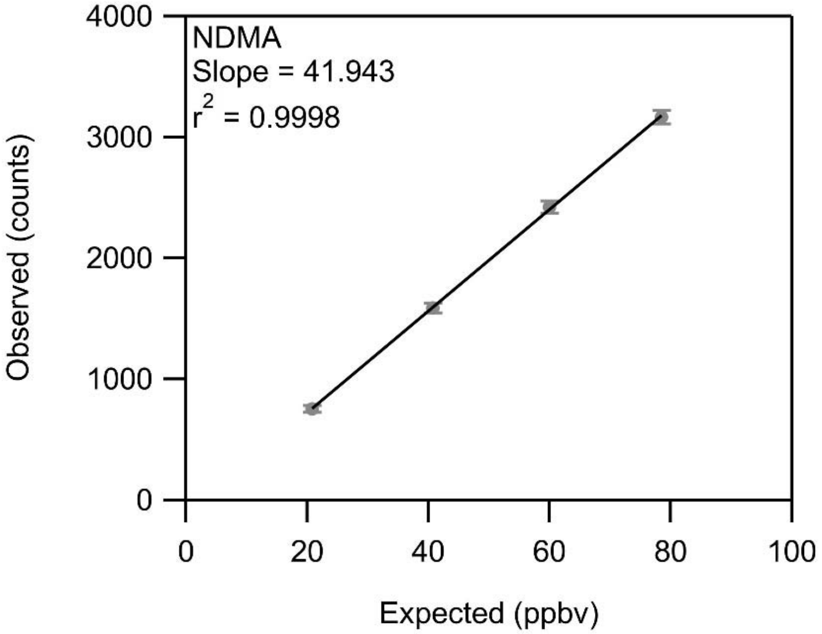

Figure 5-31. Correlation Between the Observed Signal and Expected Concentration of NDMA.

5.6.13 Benzene (m/z 78)

Figure 5-32 shows the mass spectra of benzene during H_3O^+ and NO^+ modes. In H_3O^+ mode, the response is at m/z 79, which is the MW+1 ion as expected, and at m/z 78 in NO^+ mode. The IP of benzene is 9.24 eV, which is very close to NO (9.26 eV). When the IP is close between two species, they can form an adduct. For benzene (MW 78) and NO (MW 30), this would create an ion at m/z 108. Inspection at m/z 108 showed a response with a peak of < 2 counts. Compared to the ~50 count peak of benzene in Figure 5-31, the response of the adduct seem to be negligible. Given this, benzene is a good candidate for NO^+ mode sampling. The m/z 78 ion will be used to calculate the sensitivity of benzene.

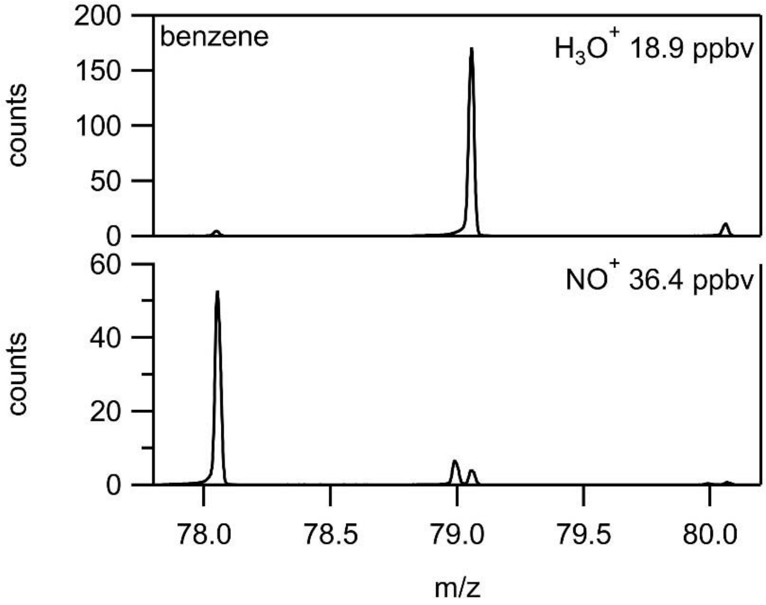

Figure 5-32. Mass Spectra of Benzene Response During H_3O^+ and NO^+ Modes.

Figure 5-33 shows the observed counts at m/z 78 during a multipoint calibration versus the calculated expected concentration. The counts shown in Figure 5-33 are a result of calculating the area under the peak shown in Figure 5-32. An r^2 of 0.999 shows a good fit and the slope of 54.431 counts/ppbv shows that benzene is sensitive enough to allow for a good response in NO^+ mode.

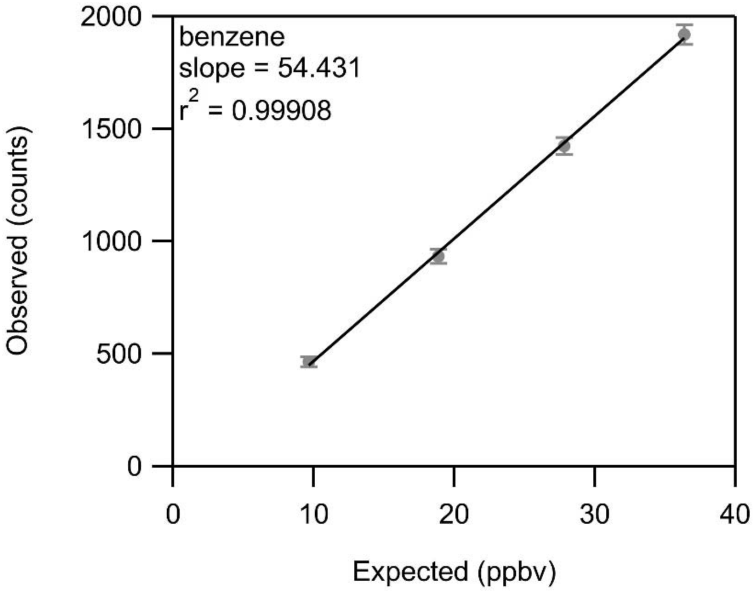

Figure 5-33. Correlation Between the Observed Signal and Expected Concentration of Benzene.

5.6.14 Diethylketone (m/z 86)

Figure 5-34 shows the mass spectra of diethylketone during H_3O^+ and NO^+ modes. In H_3O^+ mode, the response is at m/z 87, which is the MW+1 ion as expected, and at m/z 86 in NO^+ mode. The IP of diethylketone is 9.31 eV, which is very close to NO at 9.26 eV. When IP of two compounds is this close there is the chance an adduct can form, which produces a response at the sum of the MWs. In this case, an adduct would form at m/z 116 (m/z 86 + m/z 30). Figure 5-34 shows the response of diethylketone at m/z 116 in NO^+ mode and the higher signal at this ion makes it a good candidate to calculate the sensitivity of diethylketone.

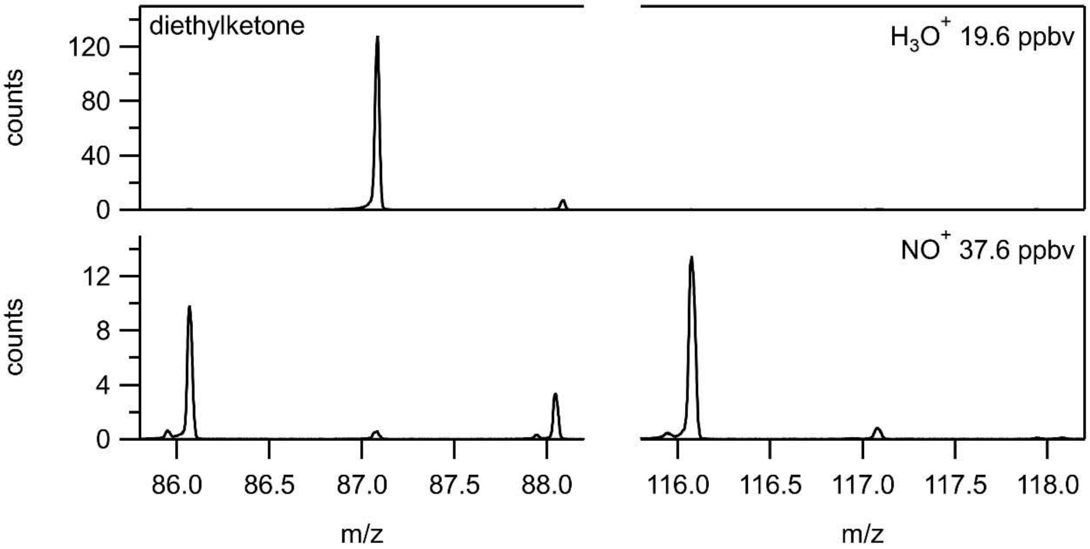

Figure 5-34. Mass Spectra of Diethylketone Response During H_3O^+ and NO^+ Modes.

Figure 5-35 shows the observed counts at m/z 86 and m/z 116 during a multipoint calibration versus the calculated expected concentration. The counts shown in Figure 5-35 are a result of calculating the area under the peaks shown in Figure 5-34. The r^2 values of 0.999 and 0.997 show a good fit at both m/z 86 and m/z 116, respectively. The slopes of 11.258 counts/ppbv for m/z 86 and 15.226 counts/ppbv for m/z 116 show that diethylketone is sensitive enough to allow for a good response in NO^+ mode and the higher sensitivity at m/z 116 makes it a better ion to observe for diethylketone quantification in NO^+ mode.

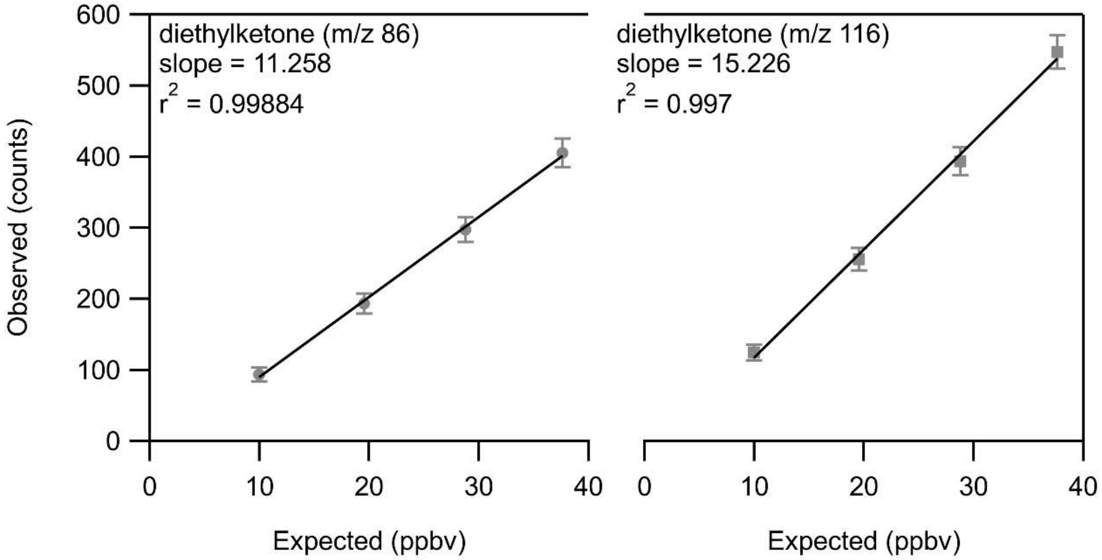

Figure 5-35. Correlation Between the Observed Signal and Expected Concentration of Diethylketone.

5.6.15 Toluene (m/z 92)

Figure 5-36 shows the mass spectra of toluene during H_3O^+ and NO^+ modes. In H_3O^+ mode, the response is at m/z 93, which is the MW+1 ion as expected, and at m/z 92 in NO^+ mode. The IP of toluene is 8.828 eV, which is lower than NO (9.26 eV) and makes it a good candidate for NO^+ mode sampling. The m/z 92 ion will be used to calculate the sensitivity of toluene.

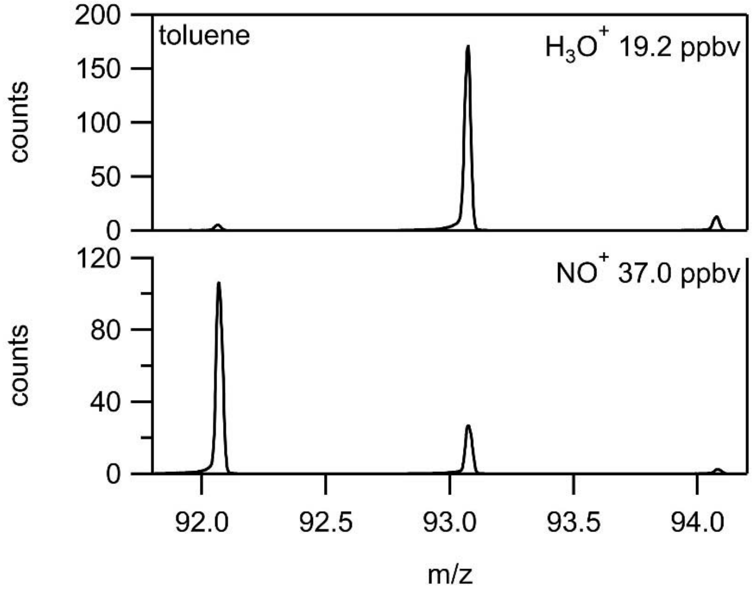

Figure 5-36. Mass Spectra of Toluene Response During H_3O^+ and NO^+ Modes.

Figure 5-37 shows the observed counts at m/z 92 during a multipoint calibration versus the calculated expected concentration. The counts shown in Figure 5-37 are a result of calculating the area under the peak shown in Figure 5-36. An r^2 of 0.999 shows a good fit and the slope of 115.41 counts/ppbv shows that toluene is sensitive enough to allow for a good response in NO^+ mode.

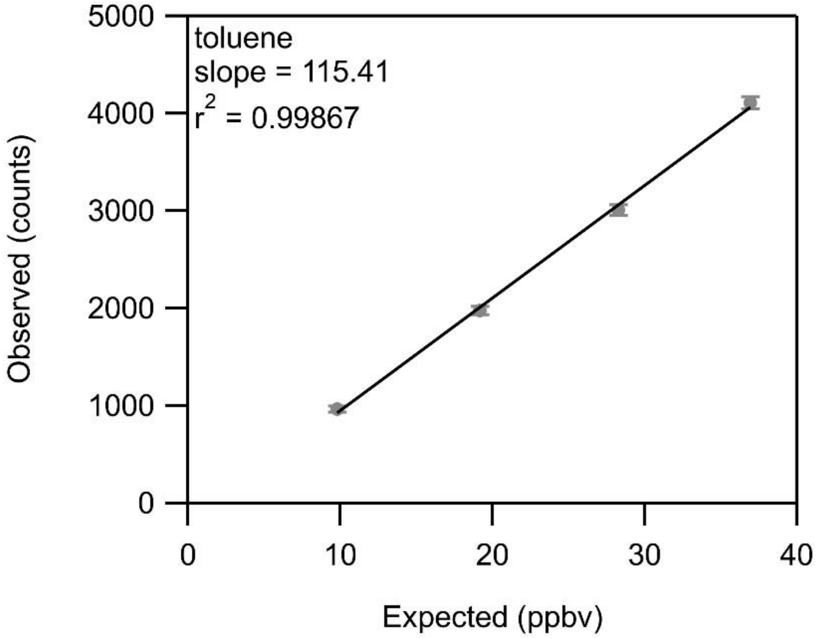

Figure 5-37. Correlation Between the Observed Signal and Expected Concentration of Toluene.

5.6.16 3-hexanone (m/z 100)

Figure 5-38 shows the mass spectra of 3-hexanone during H_3O^+ and NO^+ modes. In H_3O^+ mode, the response is at m/z 101, which is the MW+1 ion as expected, and at m/z 100 in NO^+ mode. The IP of 3-hexanone is between 9.12 and 9.3 eV, which is very close to NO at 9.26 eV. When IP of two compounds is this close, there is the chance an adduct can form, which produces a response at the sum of the MWs. In this case, an adduct would form at m/z 130 (m/z 100 + m/z 30). Figure 5-38 shows the response of 3-hexanone at m/z 130 in NO^+ mode and the higher signal at this ion makes it a good candidate to calculate the sensitivity of 3-hexanone.

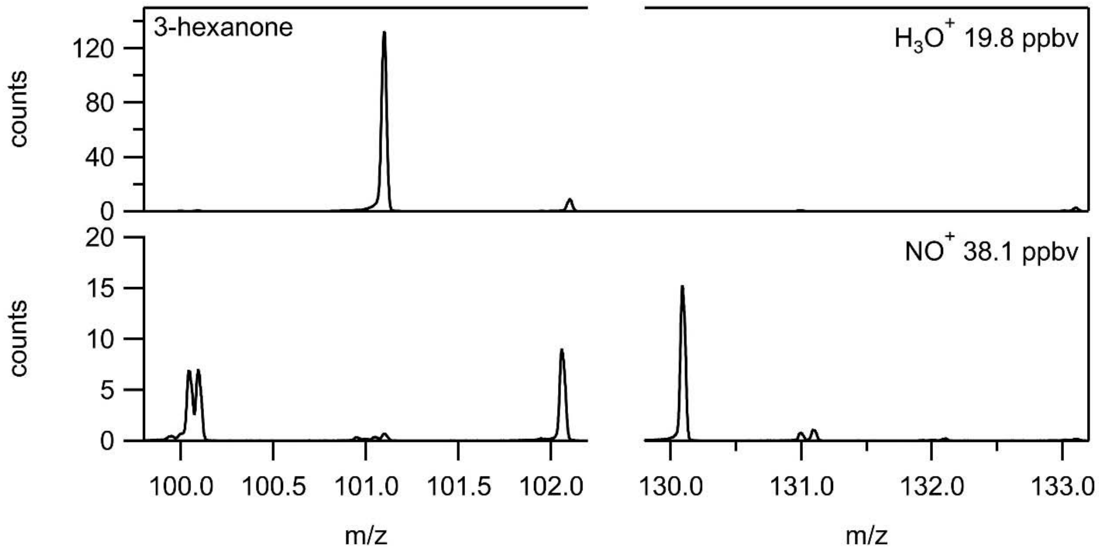

Figure 5-38. Mass Spectra of 3-hexanone Response During H_3O^+ and NO^+ Modes.

Figure 5-39 shows the observed counts at m/z 100 and m/z 130 during a multipoint calibration versus the calculated expected concentration. The counts shown in Figure 5-39 are a result of calculating the area under the peaks shown in Figure 5-38. The r^2 values of 0.998 for both m/z 100 and m/z 130 show a good fit. The slopes of 5.822 counts/ppbv for m/z 100 and 16.744 counts/ppbv for m/z 130 show that 3-hexanone is sensitive enough to allow for a good response in NO^+ mode and the higher sensitivity at m/z 130 makes it a better ion to observe for 3-hexanone quantification in NO^+ mode.

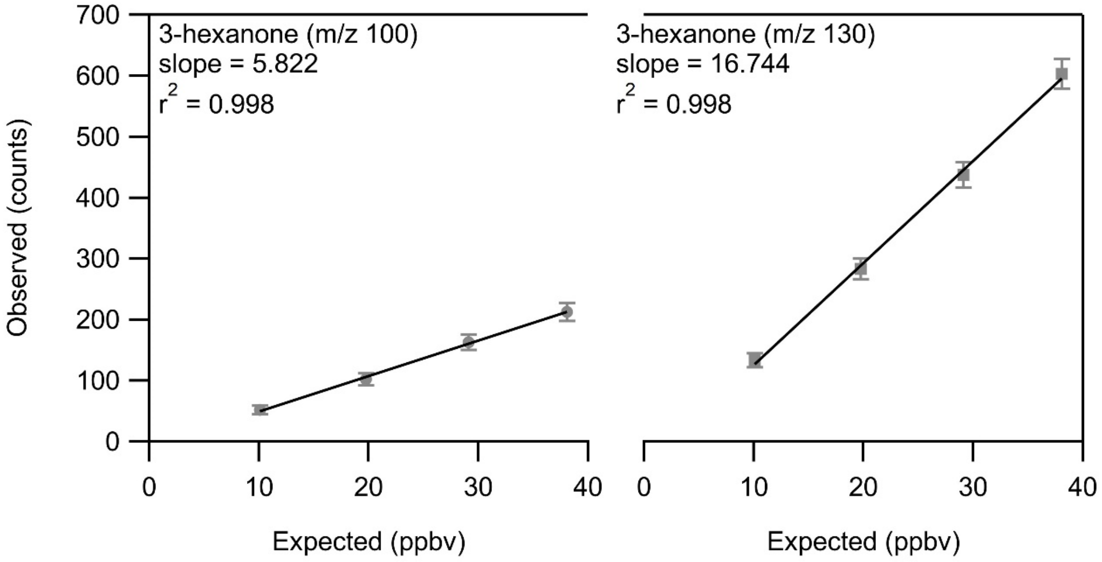

Figure 5-39. Correlation Between the Observed Signal and Expected Concentration of 3-hexanone.

5.6.17 P-xylene (m/z 106)

Figure 5-40 shows the mass spectra of p-xylene during H_3O^+ and NO^+ modes. In H_3O^+ mode, the response is at m/z 107, which is the MW+1 ion as expected, and at m/z 106 in NO^+ mode. The IP of p-xylene is 8.44 eV, which is lower than NO (9.26 eV) and makes it a good candidate for NO^+ mode sampling. The m/z 106 ion will be used to calculate the sensitivity of p-xylene.

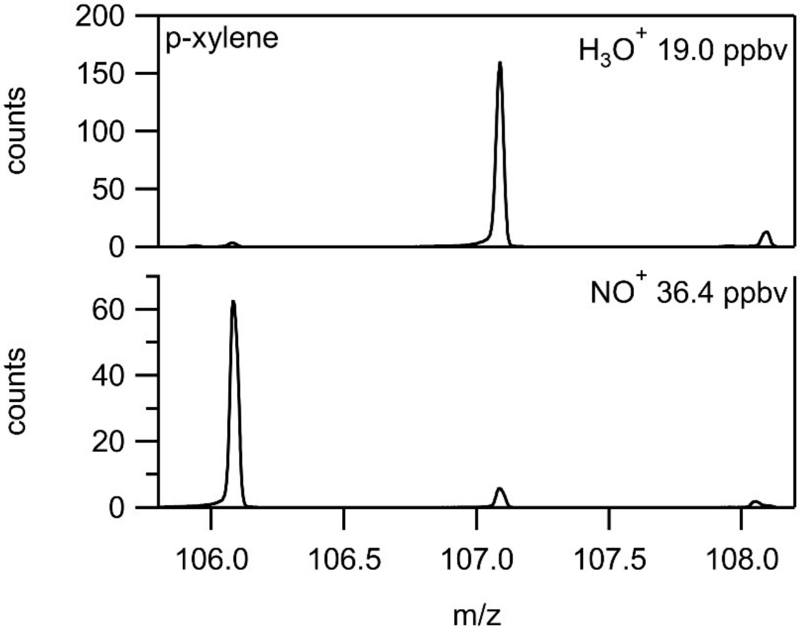

Figure 5-40. Mass Spectra of P-xylene Response During H_3O^+ and NO^+ Modes.

Figure 5-41 shows the observed counts at m/z 106 during a multipoint calibration versus the calculated expected concentration. The counts shown in Figure 5-41 are a result of calculating the area under the peak shown in Figure 5-40. An r^2 of 0.998 shows a good fit and the slope of 71.931 counts/ppbv shows that p-xylene is sensitive enough to allow for a good response in NO^+ mode. This sensitivity will be used to quantify the response for xylenes (m, p, o) and ethylbenzene.

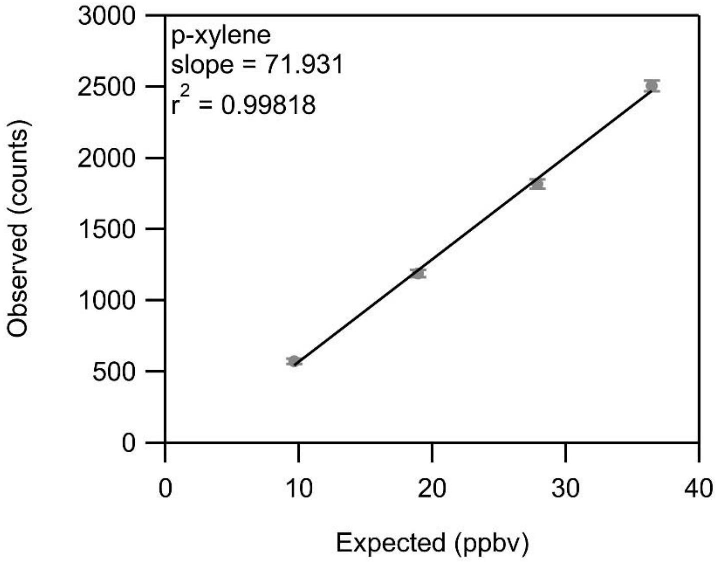

Figure 5-41. Correlation Between the Observed Signal and Expected Concentration of P-xylene.

5.6.18 1,3,5-trimethylbenzene (m/z 120)

Figure 5-42 shows the mass spectra of 1,3,5-trimethylbenzene during H_3O^+ and NO^+ modes. In H_3O^+ mode, the response is at m/z 121, which is the MW+1 ion as expected, and at m/z 120 in NO^+ mode. The IP of 1,3,5-trimethylbenzene is 8.4 eV, which is lower than NO (9.26 eV) and makes it a good candidate for NO^+ mode sampling. The m/z 120 ion will be used to calculate the sensitivity of 1,3,5-trimethylbenzene.

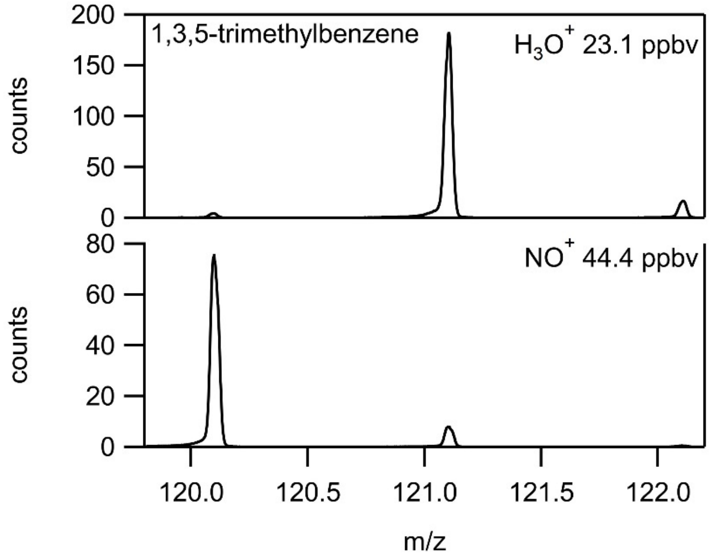

Figure 5-42. Mass Spectra of 1,3,5-trimethylbenzene Response During H_3O^+ and NO^+ Modes.

Figure 5-43 shows the observed counts at m/z 120 during a multipoint calibration versus the calculated expected concentration. The counts shown in Figure 5-43 are a result of calculating the area under the peak shown in Figure 5-42. An r^2 of 0.997 shows a good fit and the slope of 72.075 counts/ppbv shows that 1,3,5-trimethylbenzene is sensitive enough to allow for a good response in NO^+ mode. This sensitivity will be used to quantify the response for all isomers of C_3-benzenes.

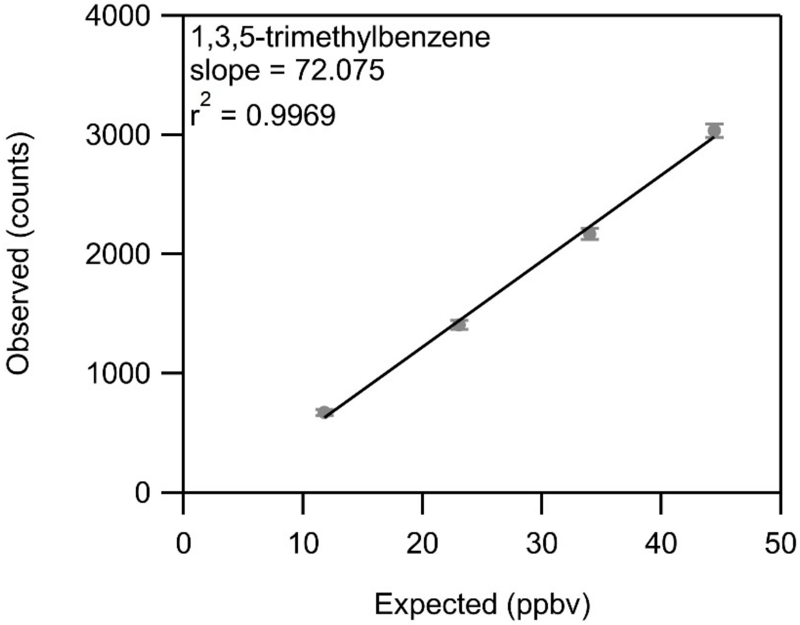

Figure 5-43. Correlation Between the Observed Signal and Expected Concentration of 1,3,5-trimethylbenzene.

5.6.19 1,2,3,5-tetramethylbenzene (m/z 134)

Figure 5-44 shows the mass spectra of 1,2,3,5-tetramethylbenzene during H_3O^+ and NO^+ modes. In H_3O^+ mode, the response is at m/z 135, which is the MW+1 ion as expected, and at m/z 134 in NO^+ mode. The IP of 1,2,3,5-tetramethylbenzene is between 8.07 and 8.47 eV, which is lower than NO (9.26 eV) and makes it a good candidate for NO^+ mode sampling. The m/z 134 ion will be used to calculate the sensitivity of 1,2,3,5-tetramethylbenzene.

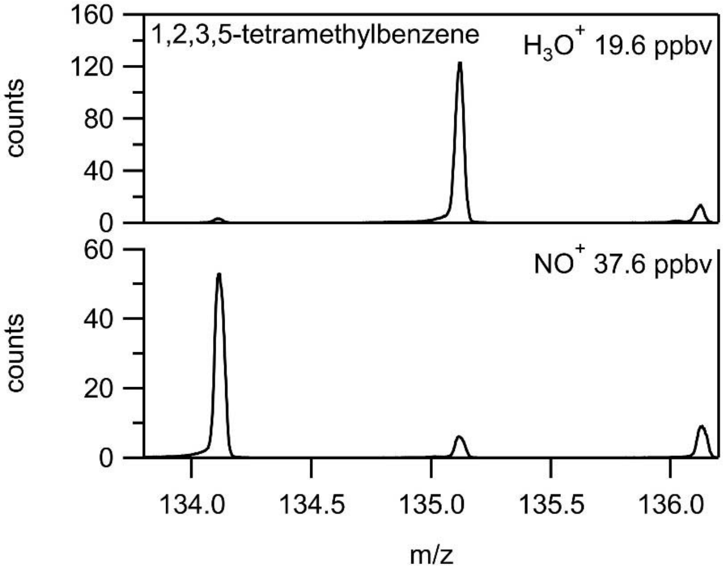

Figure 5-44. Mass Spectra of 1,2,3,5-tetramethylbenzene Response During H_3O^+ and NO^+ Modes.

Figure 5-45 shows the observed counts at m/z 134 during a multipoint calibration versus the calculated expected concentration. The counts shown in Figure 5-45 are a result of calculating the area under the peak shown in Figure 5-44. An r^2 of 0.994 shows a good fit and the slope of 52.032 counts/ppbv shows that 1,2,3,5-tetramethylbenzene is sensitive enough to allow for a good response in NO^+ mode. This sensitivity will be used to quantify the response for all isomers of C_4-benzenes.

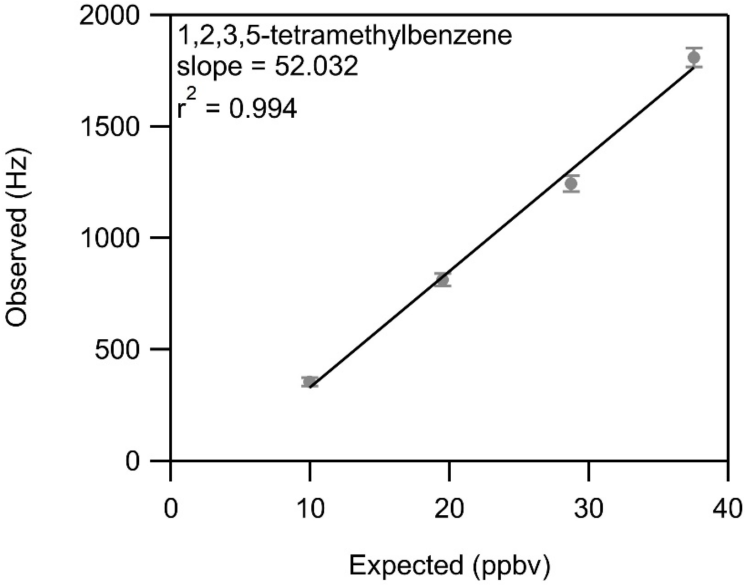

Figure 5-45. Correlation Between the Observed Signal and Expected Concentration of 1,2,3,5-Tetramethylbenzene.

5.6.20 Alpha-pinene (m/z 136)

Figure 5-46 shows the mass spectra of alpha-pinene during H_3O^+ and NO^+ modes. In H_3O^+ mode, the response is at m/z 137, which is the MW+1 ion as expected, and at m/z 136 in NO^+ mode. The IP of alpha-pinene is 8.07 eV, which is lower than NO (9.26 eV) and makes it a good candidate for NO^+ mode sampling. The m/z 136 ion will be used to calculate the sensitivity of alpha-pinene.

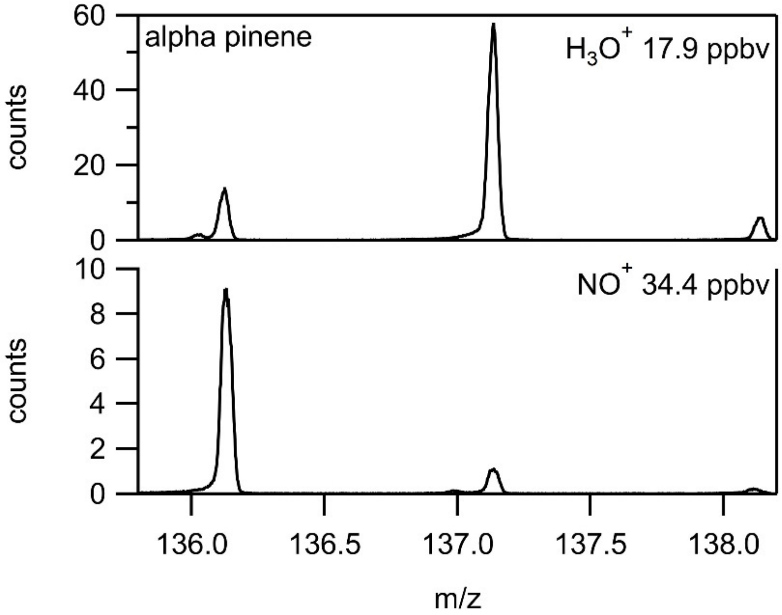

Figure 5-46. Mass Spectra of Alpha-pinene Response During H_3O^+ and NO^+ Modes.

Figure 5-47 shows the observed counts at m/z 136 during a multipoint calibration versus the calculated expected concentration. The counts shown in Figure 5-47 are a result of calculating the area under the peak shown in Figure 5-46. An r^2 of 0.999 shows a good fit and the slope of 9.285 counts/ppbv shows that alpha-pinene is sensitive enough to allow for a good response in NO^+ mode. This sensitivity will be used to quantify monoterpenes that respond at this ion.

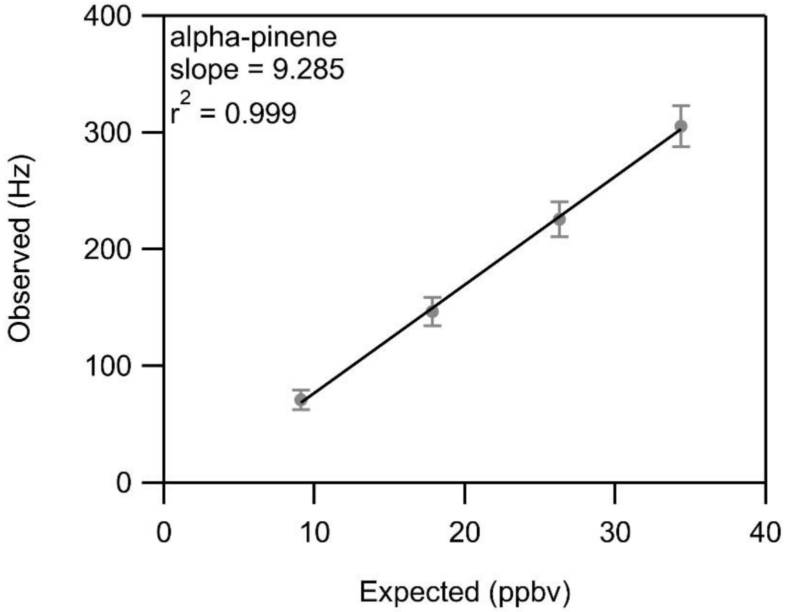

Figure 5-47. Correlation Between the Observed Signal and Expected Concentration of Alpha-pinene.

5.7 Calibration Factor Summary

Table 5-4 is a summary of the calibration factors presented above. Of the 20 species analyzed, 13 of them are sensitive enough to allow for good quantification. The species in red will not be analyzed in NO^+ mode due to their low IP.

Table 5-4. NO$^+$ Mode Calibration Factors for Select Species.

Species	m/z	Calibration Factor
methanol	32	N/A
acetonitrile	41	N/A
acetaldehyde	44	N/A
1,3-butadiene	54	28.85
1-butene	56	N/A
acetone	58	N/A
dimethylsulfide	62	32.52
Furan	68a	59.34
isoprene	68b	26.70
methyl vinyl ketone	70	N/A
methyl ethyl ketone	72	N/A
NDMA	74	41.94
benzene	78	54.43
Diethylketone	116	15.226
Toluene	92	115.41
3-hexanone	130	16.744
p-xylene	106	71.93
1,3,5-trimethylbenzene	120	72.08
1,2,3,5-tetramethylbenzene	134	52.03
alpha pinene	136	9.29

5.8 Maintenance Activities

During Month 4, there were 26 days spent on maintenance-related activities for the ML. These activities included vehicle maintenance, modifications to both the interior and exterior of the ML, and providing continuous training for ML operators. All activities were performed to improve the ML’s function and overall data collection capabilities.

Table 5-5. Mobile Laboratory Activities Performed in Month 4. (2 Sheets)

Week	Date	Description	Activities/Observations
15	11/12/2018	ML Maintenance	ML Operator DAQFactory training.
	11/13/2018	ML Maintenance	ML Operator DAQFactory training.
	11/14/2018	ML Maintenance	Heater and UPS (power supply) testing.
	11/15/2018	Stack Monitoring	Area monitoring around AP Stack to prepare for the ammonia releases in Week 16.
16	11/21/2018	ML Maintenance	Cummins®[9] generator maintenance.
17	11/26/2018	ML Maintenance	Les Schwab®[10] winter tire installation, Quality Assurance surveillance.
	11/27/2018	ML Maintenance	Instrument verification and Picarro specifications.
	11/29/2018	ML Maintenance	New deflector shield installation, exhaust temperature, tail light replacement.
	11/30/2018	ML Maintenance	ML personnel training, circuit/breaker 21 testing; measuring resistance.
18	12/03/2018	ML Maintenance	5,000-mile vehicle maintenance at McCurley®[11] Integrity Dealership; shutdown and startup procedures.
	12/04/2018	ML Maintenance and Training	Temperature controller and PTR-MS training and DAQFactory communication coding.
	12/05/2018	ML Maintenance	DAQFactory/Picarro communication coding, NO^+ mode testing, temperature controller training.
	12/06/2018	ML Testing	NO^+ mode testing.
	12/07/2018	ML Maintenance and Testing	DAQFactory/Picarro communication configurations, rack assembled, NO^+ mode testing.
19	12/10/2018	ML Maintenance and Testing	Assembled rack, NO^+ mode testing.
	12/11/2018	ML Maintenance and Testing	Assembled rack, NO^+ mode testing.
	12/12/2018	ML Maintenance and Testing	SRI testing, heated line testing and modifications.
	12/13/2018	ML Maintenance and Testing	Rack installation, Instrument software programming, heated line testing.
	12/14/2018	ML Maintenance and Testing	Instrument software programming, constructing box for temperature controllers.

---

[9] Cummins is a registered trademark of Cummins, Inc., Columbus, Indiana.
[10] Les Schwab is a registered trademark of Les Schwab Warehouse Center, Inc., Bend, Oregon.
[11] McCurley is a registered trademark of McCurley Integrity Dealerships, LLC, Tri-Cities, Washington.

Table 5-5. Mobile Laboratory Activities Performed in Month 4. (2 Sheets)

Week	Date	Description	Activities/Observations
20	12/17/2018	ML modifications	Instrument software programming and LabVIEW®[12] software installation.
	12/18/2018	ML Modifications and Training	Instrument software programming, sampling and calibration system training, construction of temperature controller box.
	12/19/2018	ML Modifications and Training	Instrument software programming, calibration system training, construction of temperature controller box.
	12/20/2018	ML Modifications and Training	Instrument software programming, calibration system training, construction of temperature controller box.
	12/21/2018	ML Modifications	Instrument software programming; changed computers to the same IP range. Began wiring of temperature controller box and prepped for new heated line system.
21	12/26/2018	ML Modifications and Testing	Instrument software programming between PTR-MS and DAQFactory; contacted Picarro and IONICON for support.
	12/27/2018	ML Modifications	Instrument software programming between PTR-MS and DAQFactory; connected to a switch. PTR-MS and DAQFactory successfully connected.
	12/28/2018	ML Modifications and Testing	Instrument software programming between PTR-MS and DAQFactory, installed pumps, installed temperature controller box, moved Variacs®[13] and pumps.

---

[12] LabVIEW is a registered trademark of National Instruments Corporation, Austin, Texas.
[13] Variac is a registered trademark of Instrument Service & Equipment, Inc., Cleveland, Ohio.

6.0 QUALITY ASSESSMENT

During the November 12, 2018, to December 31, 2018, monitoring campaign, quality control procedures were followed by the TerraGraphics Vapor Team: Data Collection and Data Processing. Data were collected and quality documents completed according to Procedure 66409-RPT-004. All data were accepted, processed, and reported according to the Procedure 17124-DOE-HS-102, "Mobile Laboratory Data Processing – Analysis." All exceptions have been noted and any potential quality-affecting issues were resolved prior to this report or are noted in this report. All potential quality-affecting deviations have been captured in Deficiency Reports (DRs) and are summarized below with some interpretation.

During the November 12, 2018, to December 31, 2018, monitoring campaign, there was one DR. DR18-012 records the issue of Variac TC-05 in the ML not receiving power and tripping a breaker.

6.1 Lessons Learned – DR18-012

On November 26, 2018, testing of TC-05, Variac TC-05, and circuit 21 was performed to determine the reason they were not receiving power. The ML personnel discovered that circuit breaker 21 was tripped. After resetting the breaker, the components were tested again. Breaker 21 tripped again which caused TC-05 and Variac TC-05 to lose power. After various tests with other Variacs, breaker 21 still tripped. In-house electrical engineers are currently helping to develop a long-term solution. Until circuit 21 is fixed, TC-05 will be heated through a different Variac on another circuit, that also heats TC-03. Circuit 21 will be tagged out until a solution is found.

7.0 CONCLUSION AND RECOMMENDATIONS

The ML was assigned to the following tank farm related tasks:

- Source Characterization of septic tanks, and
- Mobile Area Monitoring in support of the AP Stack ammonia releases.

There were no off-site activities involving the ML during Month 4.

8.0 REFERENCES

17124-DOE-HS-102, 2018, “Mobile Laboratory Data Processing – Analysis,” Revision 0, TerraGraphics Environmental Engineering, Inc., Pasco, Washington.

53005-81-RPT-027, 2018, *PTR-MS Mobile Laboratory Vapor Monitoring Monthly Report – Month 2*, Revision A, TerraGraphics Environmental Engineering, Inc., Pasco, Washington.

66409-18-ML-003, 2018, *Sampling Manifold Sketch*, TerraGraphics Environmental Engineering, Inc., Pasco, Washington.

66409-18-ML-004, 2018, *Mobile Lab Schematics*, TerraGraphics Environmental Engineering, Inc., Pasco, Washington.

66409-RPT-003, 2018, *Mobile Laboratory Operational Acceptance Testing Plan*, Revision 0, TerraGraphics Environmental Engineering, Inc., Pasco, Washington.

66409-RPT-004, 2018, *Mobile Laboratory Operational Procedure.* Revision 9, TerraGraphics Environmental Engineering, Inc., Pasco, Washington.

DR18-012, 2018, “Deficiency Report,” Rev. 0, TerraGraphics Environmental Engineering, Inc, Pasco, Washington.

Fiscal Year 2017 Mobile Laboratory Vapor Monitoring at the Hanford Site: Monitoring During Waste Disturbing Activities and Background Study, 2017, RJ Lee Group, Inc., Pasco, Washington.

Perraud, V., Meinardi, S., Blake, D.R., Finlayson-Pitts, B.J.: *Challenges Associated with the Sampling and Analysis of Organosulfur Compounds in Air Using Real-time PTR-TOF-MS and Offline GC-FID*, Atmos. Meas. Tech, 9, 1325-1340, 2016. Doi:10.5194/amt-9-1325-2016.